



Article

Phyto-Mediated Green Synthesis of Silver Nanoparticles Using an Aqueous Leaf Extract of *Momordica cymbalaria*: Antioxidant, Cytotoxic, Antibacterial, and Photocatalytic Properties

Madasamy Sundar ¹, Gopalan Rajagopal ², Ambikapathi Nivetha ³, Seetharaman Prabu Kumar ^{4,*}
and Selvaraj Muthukumar ^{1,*}

- ¹ Centre for Research and Postgraduate Studies in Botany, Ayya Nadar Janaki Ammal College (Affiliated to Madurai Kamaraj University, Madurai), Sivakasi 626124, Tamil Nadu, India; sundarcrpb@gmail.com
- ² Postgraduate and Research Department of Zoology, Ayya Nadar Janaki Ammal College (Affiliated to Madurai Kamaraj University, Madurai), Sivakasi 626124, Tamil Nadu, India; rajagopalzoology@gmail.com
- ³ Post Graduate and Research Department of Chemistry, Kongunadu Arts and Science College, Coimbatore 641029, Tamilnadu, India; nivethaambikapathi@gmail.com
- ⁴ Laboratory of Functional Molecules and Materials, School of Physics and Optoelectronic Engineering, Shandong University of Technology, Xincun West Road 266, Zibo 255000, China
- * Correspondence: drspk1989@gmail.com (S.P.K.); muthukumargowsic@gmail.com (S.M.)

Abstract: In this study, we biosynthesized the stable silver nanoparticles (AgNPs) from *Momordica cymbalaria* leaves to evaluate their antioxidant, antibacterial, cytotoxic, and photocatalytic properties. Initially, we screened the bioactive compounds from *M. cymbalaria* extract using GC-MS. The biosynthesis of *Mc*-AgNPs was confirmed using instruments, such as UV-visible spectroscopy FT-IR, XRD, SEM with EDX, and HR-TEM analyses. The UV-visible spectrum indicated absorbance at 425 nm. The crystallite size of the *M. cymbalaria*-stabilized nanoparticles was determined to be 20.14 nm. The morphology and size of the synthesized *Mc*-AgNPs were confirmed via SEM-EDX and HR-TEM analyses, with a size range from 16 to 22 nm. The synthesized *Mc*-AgNPs exhibited a photocatalytic yield of 60%. The biosynthesized *Mc*-AgNPs demonstrated strong antioxidant properties and prominent antibacterial activity against human pathogenic bacteria. The cytotoxicity study revealed that *Mc*-AgNPs were effective against MCF-7 cells in a dose-dependent manner. The recognized bioactivities confirm that the synthesized *Mc*-AgNPs act as effective catalysts in oxidation and serve as potent antioxidant, anticancer, and antibacterial agents.

Keywords: *M. cymbalaria*; silver nanoparticle; antioxidant; antibacterial; anticancer and photocatalytic activity



Citation: Sundar, M.; Rajagopal, G.; Nivetha, A.; Prabu Kumar, S.; Muthukumar, S. Phyto-Mediated Green Synthesis of Silver Nanoparticles Using an Aqueous Leaf Extract of *Momordica cymbalaria*: Antioxidant, Cytotoxic, Antibacterial, and Photocatalytic Properties. *Separations* **2024**, *11*, 61. <https://doi.org/10.3390/separations11020061>

Academic Editor: Alessandra Bonamore

Received: 28 December 2023
Revised: 8 February 2024
Accepted: 14 February 2024
Published: 17 February 2024



Copyright: © 2024 by the authors. Licensee MDPI, Basel, Switzerland. This article is an open access article distributed under the terms and conditions of the Creative Commons Attribution (CC BY) license (<https://creativecommons.org/licenses/by/4.0/>).

1. Introduction

Nanotechnology has evolved into a significant and intriguing field of research due to its unique characteristics and wide range of applications in sectors, such as agriculture, food, and health [1]. A different approach to addressing some of the most urgent issues facing the world today, such as cancer and multi-drug resistance (MDR), is Nanotherapy. When a microbe naturally becomes resistant to an antibiotic that was once useful for treating infections it caused, this is known as multi-drug resistance (MDR) [2]. With the few antimicrobial drugs now on the market, treating these drug-resistant bacterial strains, also known as “superbugs”, is quite challenging. According to Shankar (2016), if appropriate measures are not taken to address this problem, multi-drug resistance (MDR) is predicted to claim up to 10 million lives by 2050, with over 4 million of those fatalities occurring in Asia [3]. Therefore, the World Health Organization (WHO) has asked researchers worldwide to perform research and create innovative anti-MDR agents, particularly antibacterial medications, to solve this exceedingly worrisome topic [4].

Cancer is another serious illness that has long plagued humanity and stands out as one of the deadliest diseases in the contemporary world. Among women, breast cancer has consistently ranked as a prominent contributor to mortality. According to their report, the World Health Organization (WHO) anticipates a staggering 16.3 million fatalities from these ailments by 2040 [5]. Most cancer treatments and controls include surgery, chemotherapy, targeted therapy, immunotherapy, radiation therapy, and hormone therapy. Traditional therapy may cause drug resistance, recurrence, metastasis, and toxicity. Nanotechnology in medicine has offered hope to biological and therapeutic fields [6–8]. While surgery, radiation, and chemotherapy are effective conventional cancer treatments, their severe side effects lower patients' quality of life. In addition, the patient might potentially acquire resistance to MDR strains posing severe hurdles in treating cancer [9]. The development of novel treatments utilizing nanotechnology has the potential to enhance the inadequacies of existing cancer treatments.

Due to their intense color and persistent breakdown, synthetic dyes used in plastic, food, paper, paint, and cosmetics pollute the environment [10]. Most of the standard procedures to address this contamination, including reverse osmosis, coagulation, adsorption and ultra-filtration, etc., fail to decolorize and mineralize these dyes due to their high stability and complicated aromatic structures [11]. Thus, a new treatment approach is needed to destroy and deprive these crucial hazardous chemicals or convert them into environmentally friendly products [12]. Metal nanoparticles act as catalysts in several chemical processes in nano-catalysis, a fast-growing nanotechnology field [13].

Nanoparticles exhibit potential as antibiotics, antioxidants, and anticancer agents due to their small size, large surface-area-to-volume ratio, and diverse optical, chemical, magnetic, and mechanical properties [14]. Noble metal nanoparticles, such as those made from zinc, silver, copper, gold, platinum, magnesium, and titanium, have received considerable attention in biological applications due to their multifunctional diagnostics [15]. While recent advances in nanotechnology and the increasing use of nanoparticles have brought attention to previously untapped natural resources, they have also highlighted cutting-edge methods for exploiting them. The physical and chemical processes for synthesizing nanoparticles are widely known [16]. However, these techniques often produce toxic by-products during synthesis. Consequently, researchers are exploring natural biological resources, such as microbes, amino acids, polymers, sugars, vitamins, and plant extracts, to rapidly and efficiently fabricate metal nanoparticles [17,18].

Plant-mediated nanoparticle synthesis is gaining importance due to its low toxicity, efficiency, eco-friendliness, and shorter processing times [19]. This exploration into plant-based nano-synthesis delves into the diverse range of plants employed, highlighting their unique phytochemical compositions and properties. Medicinal plants' leaves, stems, and roots and the seeds and fruits of crops are harnessed to create a sustainable platform for nanomaterial synthesis. These green-synthesized nanoparticles show promise across multiple applications, driven by their biocompatibility, tunable physicochemical properties, and renewable sources [20,21]. Plants provide a rich source of bioactive compounds that can reduce, stabilize, and cap metabolites, converting metal ions into nanoparticles. This can lead to the synthesis of nanoparticles with predefined characteristics, such as flavolin, polysaccharides, alkaloid amines, proteins, terpenoids, polyphenols, tannins, and aldehydes [22].

M. cymbalaria has been used in various Asian herbal medicine systems for an extended duration [23]. *Momordica* plants are known for their biologically active compounds [24]. The identified alkaloids, flavonoids, and saponins are particularly noteworthy, as these compounds have been associated with a range of beneficial biological activities. Alkaloids, for instance, are known for their antimicrobial and anticancer properties [25]. Flavonoids are recognized for their antioxidant and anti-inflammatory effects, contributing to potential health benefits [26]. Saponins, on the other hand, have demonstrated antidiabetic properties in various studies [26]. The potential biological benefits of phytochemicals found in *Momordica* have attracted significant interest in recent studies, focusing on compounds

related to diabetes mellitus, cardioprotective properties, cancer, ulcers, and diabetic neuropathy [27–30]. It has also been documented that the herb possesses wound-healing, hypoglycemic, hypolipidemic, anti-infertility, nephroprotective, hepatoprotective, and antioxidant properties [31–35].

Silver nanoparticles (AgNPs) have emerged as a leading type among biosynthesized metal nanoparticles over the past two decades due to their distinct physical, chemical, and biological properties [36]. While AgNO₃ can be toxic at high concentrations, studies have demonstrated increased catalytic activity, chemical stability, biocompatibility, and therapeutic potential at lower concentrations of AgNO₃ [37]. The potential anti-cancer and antibacterial actions of silver nanoparticles are well-documented [38], with the controlled release of silver being a notable advantage over bulk metals and their salts [39]. The concept of new-age bio-nano formulations espouses nanotechnology with traditional medicine [40,41]. Many studies have highlighted the green synthesis of AgNPs with plant leaves, but there has been limited exploration of green synthesis using wild and native plant species with biomedical applications [42–45]. Silver nanoparticles have shown considerable promise in counteracting reactive oxygen species, indicating a potential role in reducing oxidative stress [46]. Their selective cytotoxicity against cancer cells also ignites interest in their anti-cancer mechanisms, leading to the development of novel, targeted cancer treatments [47,48]. Moreover, the broad-spectrum antimicrobial effectiveness of silver nanoparticles against a variety of pathogens underscores their importance in tackling infectious diseases and antibiotic resistance [49]. This extensive study aims to decipher the complex molecular mechanisms underlying these critical aspects, offering a comprehensive view of silver nanoparticles' therapeutic prospects and aiding progress in nanomedicine [50]. The aforementioned points indicate that synthesizing metal nanoparticles using a green chemical approach is an intriguing and underexplored opportunity, which has sparked interest in the current study.

This research examines the antibacterial, cytotoxic, and photocatalytic potential of *M. cymbalaria*-mediated silver nanoparticle synthesis. By integrating the properties of the *Momordica* genus with nanotechnology, this study seeks to demonstrate the potential applications of these nanoparticles in various medicinal and environmental contexts. Exploring green synthesis using wild species and native plants, particularly those with anti-cancer and antibacterial activities, represents a novel and underexplored opportunity, potentially leading to new insights and applications in nanomedicine and environmental sustainability.

2. Materials and Methods

Most of the chemicals utilized in this investigation were procured from various suppliers. All analytical-grade experimental chemicals were obtained from HI Media, located in Mumbai, India. These included Muller Hinton agar, Nutrient broth, Modified Eagle Medium (MEM), fetal bovine serum (FBS), trypsin, silver nitrate (AgNO₃), iodine, potassium iodide, magnesium ribbon, lead acetate, chloroform, concentrated sulfuric acid (Conc. H₂SO₄), potassium sodium tartrate, sodium hydroxide (NaOH), methanol, glacial acetic acid, ferric chloride (FeCl₃), dimethyl sulfoxide (DMSO), and hydrochloric acid (HCl). Additionally, two specific chemicals, 2,2 diphenyl 1 picrylhydrazyl (DPPH) and 3-(4,5-dimethylthiazol-2-yl)-2,5-diphenyl tetrazolium bromide (MTT), were purchased from Sigma Aldrich in Bangalore, India.

2.1. Preparation of Plant Extract

M. cymbalaria plant leaves were collected from Srivilliputtur, Tamil Nadu, India. Upon collection, the plants were immediately placed in sterilized Ziplock bags and transported to the laboratory. The specimens were authenticated by taxonomists at the Centre for Research and Postgraduate Studies in Botany, Ayya Nadar Janaki Ammal College, Sivakasi, Tamil Nadu, India. The leaves were then selected for further processing. To prepare the leaf samples, they were initially rinsed with water and subsequently left to dry under a sunshade. Once dried, the leaves were ground into a fine powder. For the extraction

process, 10 g of this powdered *M. cymbalaria* leaves was steeped in conical flasks containing 100 mL of double-distilled water. The mixture was agitated thoroughly and left undisturbed for five hours to ensure sufficient extraction. Following the extraction, the solution was filtered through a Whatman No. 1 filter paper to obtain a clear filtrate, which was then used to synthesize the *Mc*-AgNPs.

2.2. Phytochemical Analysis

The crude leaf extracts of *M. cymbalaria* were subjected to qualitative analysis to detect the presence of phytochemicals. Phytoconstituents, such as alkaloids [51], flavonoids [52], carbohydrates [53], phenols, and tannins [54], along with steroids, cardiac glycosides [55], terpenoids, and phlobatannins [56], were analyzed using the following established standard procedures.

2.3. Gas Chromatography-Mass Spectrometry (GC-MS) Analysis

Chemical analysis of the *M. cymbalaria* leaf extract was performed using a Gas Chromatography-Mass Spectrometry (GC-MS, Shimadzu, Tokyo, Japan) system equipped with a Thermal Desorption (TD) unit. The GC-MS apparatus featured an Rtx-5 capillary column (30 m × 0.25 mm, with a film thickness of 0.25 μm) and employed helium as the carrier gas at a constant flow rate of 1.21 mL/min. The oven temperature was programmed to rise from 60 °C to 200 °C at a rate of 5 °C per minute before a final ramp to 280 °C. Scans were carried out at *m/z* values ranging from 50 to 450. The mass fragmentation patterns of the compounds were identified using the NIST library, with the mass spectrometer operating at 70 eV.

2.4. Synthesis of AgNPs from *M. cymbalaria*

Silver nitrate served as the precursor for the synthesis of AgNPs. As detailed in a previous report, a 1 mM AgNO₃ solution (100 mL) was prepared by dissolving the silver nitrate in deionized water. This solution was then combined with the *M. cymbalaria* leaf extract at a 2:10 ratio and incubated in a dark area. After incubation, the sample was centrifuged at 10,000 × *g* rpm for 15 min at 4 °C to obtain a clear supernatant. The resulting pellet was washed three times with deionized water [57].

2.5. Characterization of *Mc*-AgNPs

2.5.1. UV-Vis Spectroscopy

A noticeable color change occurred after incubating the *M. cymbalaria* (*Mc*) aqueous extract with the AgNO₃ solution. UV-visible spectroscopy (Shimadzu, Japan) was utilized to analyze the peaks of *Mc*-AgNPs within the wavelength range of 200 to 800 nm.

2.5.2. Fourier-Transform Infrared Spectroscopy (FT-IR) Analysis

The functional groups present in the green-synthesized *Mc*-AgNPs were characterized using Fourier Transform Infrared (FT-IR) spectroscopy to investigate the plant compounds responsible for the reduction of silver ions. The dried nanoparticle powders and the plant extract were mixed with KBr to form pellets, which were then analyzed with an FT-IR spectrometer (Spectrum 65, PerkinElmer, WA, USA).

2.5.3. X-ray Diffraction (XRD) Analysis

XRD analysis was conducted to determine the crystallinity, phase, and average crystallite size of the *Mc*-AgNPs. The synthesized nanoparticles were dispersed in ethanol and deposited onto a glass substrate for XRD analysis. The analysis was carried out using an Ultima IV-Rigaku diffractometer equipped with CuKα radiation ($\lambda = 1.540 \text{ \AA}$) at 45 kV and 30 mA, in Tokyo, Japan.

2.5.4. SEM and EDX Analysis

The dimensions and morphology of the *Mc*-AgNPs were analyzed using a Scanning Electron Microscope (SEM), specifically the Carl Zeiss Microscopy GmbH, EVO18 model from the Jena, Germany. To prepare the samples, the *Mc*-AgNPs were dispersed in 100% ethanol through ultrasonication. The solution was then deposited onto a glass slide and left to air-dry, allowing the solvent to evaporate completely. Subsequently, a thin layer of gold, approximately 3 nm in thickness, was sputtered onto the sample using a vacuum sputter coater. The SEM was equipped with an integrated Energy-Dispersive X-ray (EDX) analysis system (Quantax 200 with X Flash[®] 6130) to determine the elemental composition.

2.5.5. HR-TEM and SAED Analysis

The research utilized a high-resolution transmission electron microscope (HR-TEM) and the selected area diffraction pattern (SAED), specifically the JEOL-2100 model from JEOL India Pvt. Ltd., in New Delhi, India, with a magnification capability of 46,000 \times . Samples were prepared using the Formvar resin grid technique: a suspension of the synthesized nanoparticles at a weight-to-volume ratio of 0.5% was deposited onto a TEM grid coated with Formvar resin. The grid was air-dried for ten minutes before being examined. Photographs were captured to document the morphology of the nanoparticle aggregates.

2.6. DPPH-Radical-Scavenging Assay

A DPPH-radical-scavenging assay was developed to evaluate antioxidant properties by measuring the free-radical-scavenging activity. *Mc*-AgNPs were dissolved in deionized water at concentrations ranging from 200 to 1000 $\mu\text{g}/\text{mL}$. Ascorbic acid was used as a positive control. The assay commenced by mixing 0.1 mL of the *Mc*-AgNPs solution with 1 mL of a freshly prepared 0.1 mM DPPH solution in ethanol. After 20 min of vigorous shaking at room temperature, the absorbance at a wavelength of 517 nm was measured. A control sample, devoid of silver nanoparticles, was also prepared [58]. The radical-scavenging activity was calculated by measuring the reduction in DPPH absorbance using the following formula (Equation (1)):

$$\text{Scavenging effect (\%)} = \left[\frac{A_c - A_s}{A_c} \right] \times 100 \quad (1)$$

where, A_c is the abs of the control, and A_s is the abs of the sample or standard.

2.7. Cytotoxicity Assay

The MCF-7 (breast cancer) and Vero cell line (non-cancerous) were cultured in DEME medium supplemented with 10% fetal bovine serum, 100 units/mL of penicillin, and streptomycin at 37 °C with 5% CO₂ and 95% relative humidity. The culture media were replaced twice a week. The in vitro cytotoxicity activity *Mc*-AgNPs was evaluated against the MCF-7 human breast cancer cell line and Vero cell lines using the 3-(4,5-dimethylthiazol-2-yl)-2,5-diphenyl tetrazolium bromide (MTT) assay [59]. Initially, 1×10^5 cells were seeded in a 96-well plate and allowed to attach for 24 h. The previous culture medium was then replaced with a medium containing various concentrations of *Mc*-AgNPs (1.95 to 1000 $\mu\text{g}/\text{mL}$), and the assay was triplicated. Doxorubicin was used as the reference drug (0.1 g/mL). After a 24 h incubation, the cells were washed three times with $1 \times$ PBS buffer, and MTT solution (5 mg/mL) was added. Following a 2 h incubation at 37 °C, the formed formazan crystals were diluted in 1 mL of dimethylsulfoxide (DMSO), and the absorbance was measured at 570 nm using a microplate reader (BMG Labtech in Ortenberg, Germany). The percentage of viability was calculated using the following formula [60] (Equation (2)).

$$\text{Cell viability (\%)} = \left[\frac{(\text{OD}_{\text{sample}} - \text{O.D.}_{\text{blank}})}{\text{O.D.}_{\text{control}}} \right] \times 100 \quad (2)$$

2.8. Antibacterial Activity

The bacterial strains, such as methicillin-resistant *Staphylococcus aureus* ATCC-43300 (MRSA), vancomycin-resistant *Enterococcus faecium* ATCC 49624 (VREF), *Escherichia coli* ATCC-25922, and *Serratia marcescens* ATCC-27137, were obtained from the American Type Culture Collection (ATCC). Muller Hinton Agar (MHA) was used as the medium to test the antibacterial efficacy of *Mc*-AgNPs via the Kirby-Bauer well-diffusion methods. The process involved pouring sterilized MHA onto sterile Petri plates and waiting for it to solidify. After the medium was ready, bacteria were inoculated onto the surface using a sterile cotton swab. In the well-diffusion method, wells were punched into the agar using a cork borer 15 min later. *Mc*-AgNPs were introduced into three separate wells at concentrations of 50 µg/mL, 100 µg/mL, and 150 µg/mL, which were made from a stock solution dissolved in 50% DMSO. The plates were incubated at 37 °C, and the inhibition zones were measured 24 h later to evaluate the antibacterial activity of *Mc*-AgNPs [61].

Microbial Growth Assay

The assessment of the antibacterial efficacy of *Mc*-AgNPs against bacterial pathogens was conducted by subjecting 10^7 colony-forming units (CFUs) of bacterial isolates to individual treatments with varying concentrations of *Mc*-AgNPs (100, 80, 60, 40, and 20 µg/mL). Following an initial incubation period of 1 h at 30 °C, bacterial colonies were quantified using an automated colony counter [62].

2.9. Photocatalytic Activity

The photodegradation of methylene blue dye solution was investigated under sunlight in a batch reactor system, utilizing the synthesized *Mc*-AgNPs as the catalyst [63]. An open-type rectangular tray measuring 16 × 15 × 5 cm and made of borosilicate glass was employed as a reactor to sustain the dye solution in sunlight-mediated photocatalysis. Methylene blue dye (0.159 g) was dissolved in distilled water to produce a 1 molar solution of 1 L. From this, 50 mL was taken and diluted to a 250 mL solution (500 ppm). This prepared solution was transferred to the rectangular tray and *Mc*-AgNPs (50 mg or 0.05 g) were added. One molar NaOH/HCl was used to maintain a neutral pH. The mixture of the 250 mL dye solution with a known concentration and the synthesized *Mc*-AgNPs nanocomposite was stirred vigorously using a magnetic stirrer at a medium rotation to attain equilibrium. After allowing the adsorption process to equilibrate, the mixture was exposed to sunlight for 30 min. UV-visible spectroscopy was used to analyze the solution to obtain the maximum absorption range. Then, the solution was irradiated in sunlight for 180 min with continuous stirring. Initially, the irradiated dye solution was collected within 10 min, and the remaining dye solution was collected at intervals every 20 min and then analyzed using a UV-Visible spectrophotometer. The ideal conditions for the photodegradation investigation were maintained under direct sunlight. Every 30 min, the amount of solar light was monitored, and the average amount of light over the course of each experiment was computed. The UV-Vis spectrophotometer measured the residual concentration of the dye solution at 665 nm. A digital lux meter was used to measure the intensity of light and sunshine throughout the reaction time, which was around 820 lux. Throughout the studies, the intensity remained almost constant.

The formula below was used for calculating the degradation percentage (Equation (3)).

$$\% \text{ of degradation} = ((C_0 - C_t) / (C_0)) \times 100 \quad (3)$$

Where C_0 was the initial absorbance of the dye solution and C_t was the absorbance at time intervals.

2.10. Statistical Analysis

All experiments were conducted in triplicate to ensure reproducibility. Statistical analyses were performed to assess the significance of differences between the measured

mean values using a two-tailed Student's *t*-test. A *p*-value of less than 0.05 was deemed to indicate statistical significance. All statistical calculations were performed using SPSS software (version 21.0; I.B.M. Corp., New York, NY, USA).

3. Results and Discussion

The presence of diverse phytochemicals in *M. cymbalaria* underscores its potential as a valuable source of bioactive compounds in Table 1. While our results support the potential pharmacological relevance of *M. cymbalaria* extracts, it is crucial to highlight the need for further investigations, including detailed chemical isolation and mechanistic studies. Identifying the compounds responsible for the observed bioactivities would provide a more comprehensive understanding of the plant's therapeutic potential. Moreover, contrary to some previous studies, the absence of tannins in the extract warrants additional exploration to elucidate the variability in the phytoconstituent compositions among different plant samples. The phytochemical profile of *M. cymbalaria* showcases its richness in bioactive compounds, opening avenues for future research on its medicinal and therapeutic applications. However, further studies are necessary to unravel the mechanisms underlying its observed pharmacological activities.

Table 1. Preliminary phytochemical analysis of *M. cymbalaria* extract.

S.No.	Phytochemical Class	<i>M. cymbalaria</i> Leaf Extract
1	Alkaloids	++
2	Flavonoids	++
3	Tannins	–
4	Phenols	+
5	Steroids	+
6	Saponin	++
7	Terpenoids	+
8	Carbohydrates	+
9	Phlobatannins	–

++ Indicates the presence of a high amount; + indicates the presence; – indicates the absence of the phytochemical.

3.1. GC-MS Analysis

The GC-MS analysis of the leaf extract of *M. cymbalaria* leaves provided valuable insights into the composition of phytocompounds present in the plant (Figure 1 and Table 2). Oleic acid emerged as the predominant compound, constituting 39.37% of the total composition. This finding aligns with previous studies highlighting the prevalence of oleic acid in various plant extracts, showcasing its significance in plant metabolism and potential health benefits [64–66]. *n*-Hexadecanoic acid (20.86%) and octadecanoic acid (11.26%) further contributed to the fatty acid profile of the extract. Fatty acids play crucial roles in plant development and are known for their diverse physiological functions [67,68]. Additionally, the presence of 5-hydroxymethylfurfural (8.49%), known for its antioxidant properties, adds another layer of potential health benefits associated with the extract [69]. The diverse classes of compounds, including esters, steroids, fatty acids, terpenes, aliphatic alcohols, and flavonoids, suggest the complex chemical composition of *Momordica cymbalaria*, contributing to its pharmacological significance [70]. It is noteworthy that while the identified compounds provide valuable information, further research is essential to explore the specific biological activities and potential synergistic effects of these phytocompounds. Comparative studies with other *Momordica* species may reveal unique chemical signatures and therapeutic potentials. Future studies should delve into the bioactivities associated with these compounds and their practical applications in medicine and nutrition.

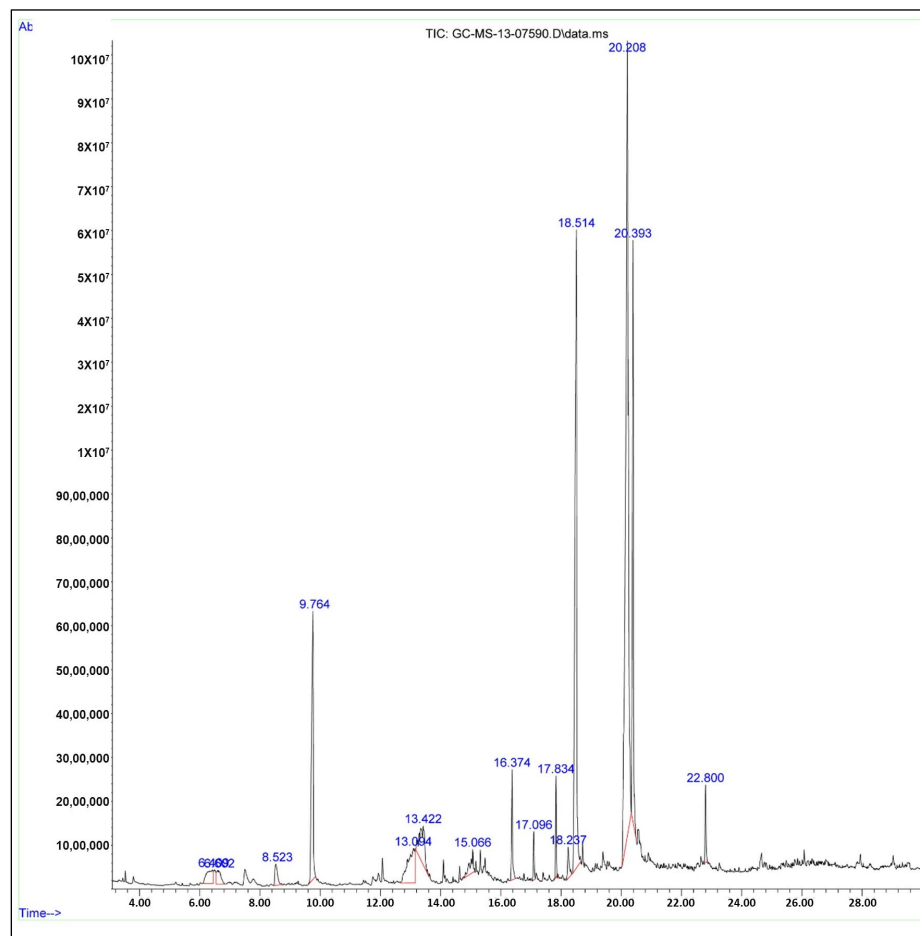


Figure 1. Analysis of bioactive compounds from *M. cymbalaria* via GC-MS.

Table 2. GC-MS profile of phytochemicals in *M. cymbalaria* extract.

Peak	R. Time	Area	Area%	Name
1	6.409	4,709,431	1.66	S-Methyl-L-cysteine, N-(ethoxyca...
2	6.602	3,217,202	1.14	S-Methyl-L-cysteine, N-(ethoxyca...
3	8.523	2,997,683	1.06	4H-Pyran-4-one, 2, 3-dihydro-3,5-...
4	9.764	24,034,843	8.49	5-Hydroxymethylfurfural
5	13.094	13,332,417	4.71	2-Isopropoxyethyl propionate
6	13.422	10,307,348	3.64	1,3-Dioxane, 4,4-dimethyl-
7	15.066	3,657,786	1.29	Humulenol-II
8	16.374	5,827,800	2.06	Tetradecanoic acid
9	17.096	2,281,005	0.81	Cyclohexanol, 3-ethenyl-3-methyl...
10	17.834	3,981,804	1.41	(3S,3aS,6R,7R,9aS)-1, 1, 7-Trimeth...
11	18.237	2,697,462	0.95	Palmitoleic acid
12	18.514	59,065,176	20.86	n-Hexadecanoic acid
13	20.208	111,488,797	39.37	Oleic Acid
14	20.393	31,876,258	11.26	Octadecanoic acid
15	22.800	3,678,672	1.30	Dehydroabietic acid

3.2. Green Synthesis of *Mc*-AgNPs

The silver nitrate was mixed with the plant extract, the silver ions from AgNO_3 bound to the plant proteins, and water-soluble compounds using $-\text{OH}$ and $-\text{COOH}$ groups, leading to conformational changes in the protein molecule, which contributed to the captured metal ion transformation into a silver nanoparticle [71]. In general, a metal nanoparticle synthesis mechanism using plants and plant extracts contains three main steps: (1) the phase of activation wherein metal ions are reduced and reduced metal atoms are nucleated; (2) the growth phase that is characterized by an increase in the thermodynamic stability of nanoparticles and the spontaneous coalescence of small adjacent nanoparticles into larger particles (direct formation of nanoparticles through heterogeneous nucleation and growth, and further metal ion reduction; a process referred to as an Ostwald ripening); (3) the final shape of the nanoparticles is determined at the process termination step.

3.3. Characterization of *Mc*-AgNPs

3.3.1. UV-Vis Spectroscopic Analysis

The aqueous leaf extract of *M. cymbalaria* was mixed with an AgNO_3 solution and initially turned into a pale yellow color. Then, after incubation at 8 h, the solution turned dark brown, indicating the synthesis of *Mc*-AgNPs. Similar observations were reported by other investigators who used plant extracts as a reducing agent [72,73]. Further, the UV-Vis spectroscopy, widely employed for identifying the structural properties of nanoparticles, revealed a distinct peak at 425 nm, indicating the broad size distribution and presence of AgNPs on the surface of the nanoparticles in the solution (Figure 2). This peak is attributed to the surface plasmon resonance of electrons [74]. The transformation of silver ions into silver nanoparticles began as soon as the reaction was initiated, with the complete reduction occurring within about two minutes at ambient conditions, which signifies the quick biosynthesis of the silver nanoparticles [75].

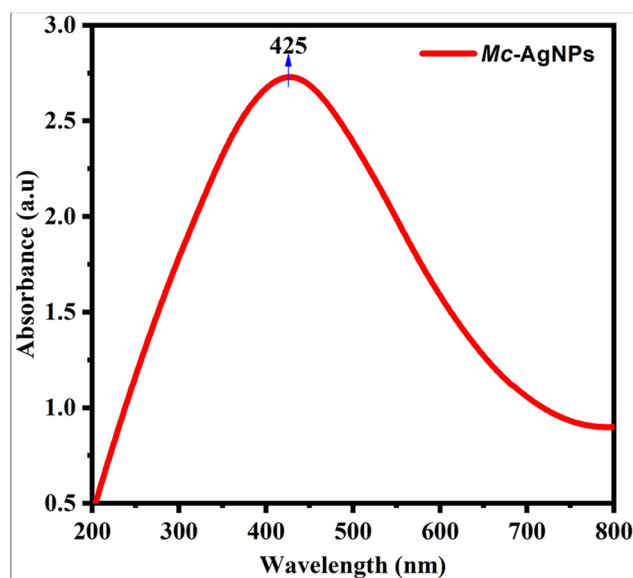


Figure 2. UV analysis of synthesized *Mc*-AgNPs. A peak of 425 nm demonstrates the production of AgNPs on the surface of nanoparticles in the solution due to the surface-plasma resonance (SPR) electrons.

3.3.2. FT-IR Analysis

The chemical composition and functional groups present in *Mc*-AgNPs were investigated using FT-IR spectroscopy. The probable biomolecules responsible for the capping and reduction of silver nanoparticles were determined using FT-IR spectroscopy. Figure 3 displays the FT-IR spectrum for the *Mc* aqueous extract and *Mc*-AgNPs. The strong and broad absorption peak observed at 3412.13 cm^{-1} represents the O-H stretching of water molecules. The characteristic peaks at 2930.79 cm^{-1} and 2854.58 cm^{-1} are attributed to

C-H stretching vibrations [14]. The peak at 2923.79 cm^{-1} corresponds to the medium C-H stretching of alkanes. The absorption at 2164.07 cm^{-1} is indicative of the strong C-N stretching of thiocyanate. The peaks at 2387.24 cm^{-1} , 2059.09 cm^{-1} , and 1745.72 cm^{-1} correspond to strong C=O stretching in the compound. The smaller peaks at 1626.27 , 1403.57 cm^{-1} , and 1654.74 cm^{-1} are credited to the medium C=C stretching of disubstituted alkenes (cis) and medium O-H bending and medium C=N stretching of imines/oximes. The functional group C=C stretching of cyclic alkenes was observed at 1563.54 cm^{-1} . The minor peaks at 1250.38 and 1118.19 cm^{-1} were strongly related to the C-O stretching of aromatic esters and aliphatic/aryl ethers, respectively. The C-N stretching of amine groups was recorded at 1160.18 cm^{-1} . The sharp peaks at 1076.20 cm^{-1} correspond to the strong C-O stretching of primary alcohols. The presence of flavanones and terpenoids in the plants are evidenced by the absorption by AgNPs, confirmed by the presence of carbonyl (C=O) groups. These carbonyl groups strongly bind to AgNPs and act as stabilizing molecules [76].

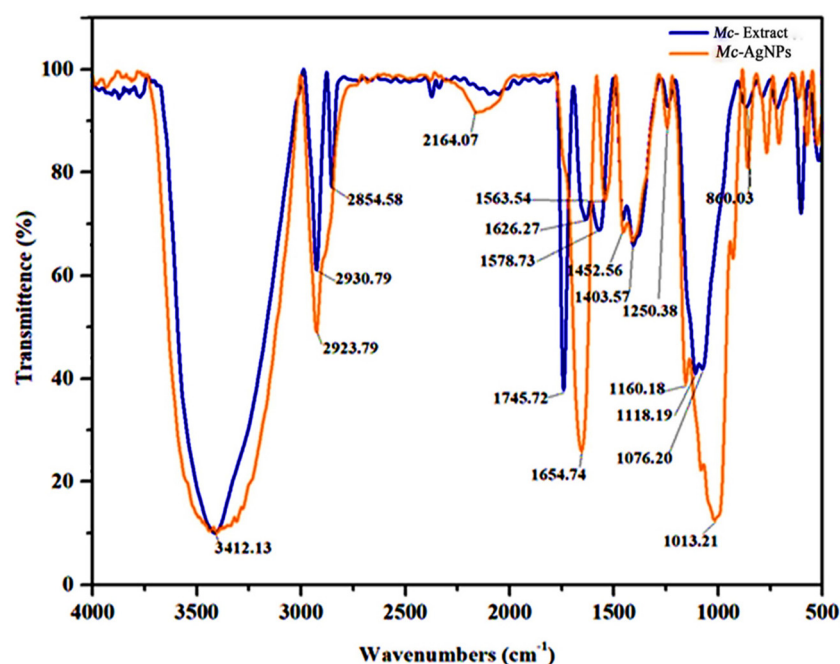


Figure 3. FT-IR spectrum of *Mc* and *Mc-AgNPs*.

3.3.3. XRD Analysis

The crystallographic characteristics of the *Mc-AgNPs* were determined through X-ray diffraction (XRD) analysis. The XRD spectrum highlighted several distinct peaks corresponding to the Bragg reflections, notably at 2θ angles of 38.15° , 44.48° , 64.56° , and 77.64° . These peaks were attributed to the (111), (200), (220), and (311) lattice planes, respectively, as shown in Figure 4. These lattice planes indicate the face-centered cubic (F.C.C.) structure, confirming the crystalline nature of the *Mc-AgNPs*, which is in alignment with the standard JCPDS card no: 84-0713. The presence of these peaks suggests that the plant-based synthesis approach yields well-defined crystalline nanoparticles, likely due to the presence of natural stabilizing compounds in the plant extracts that aid in maintaining the structural integrity of the nanoparticles. Comparative analysis suggests that the diffraction patterns of the *Mc-AgNPs* show remarkable similarity to those reported for nanoparticles synthesized using *Euphorbia antiquorum* and *Corallocarpus epigaeus*, which exhibit analogous diffraction features corresponding to the same indexed planes [77,78]. This similarity underscores a consistent crystalline structure among plant-mediated synthesized silver nanoparticles [79].

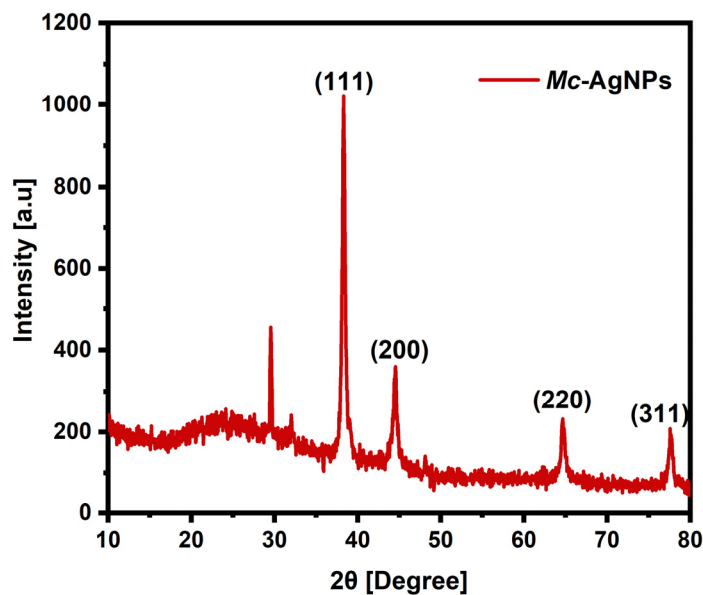


Figure 4. XRD analysis of *Mc-AgNPs*. The XRD revealed the formation of metallic Ag from Ag⁺ using the *M. cymbalaria* leaf extract.

3.3.4. SEM and E.D.X. Analysis

The SEM analysis was used to determine the size and shape of the *Mc-AgNPs*. According to the SEM analysis, the synthesized *Mc-AgNPs* had a cluster-like shape and significantly agglomerated. The SEM analysis of *Mc-AgNPs* is shown in Figure 5. Additionally, the dehydration that occurred during sample preparation for SEM analysis most likely contributed to the substantial aggregation of the biosynthesized AgNPs [80]. E.D.X. analysis determined the elemental makeup, atomic composition and weight percentage of the *Mc-AgNPs*. The E.D.X. analysis of *Mc-AgNPs* is shown in Figure 5. The study revealed certain contaminants, including carbon, oxygen, silicon, and very minute amounts of calcium and sodium. Oxygen and carbon were also present in the spectra. These elements were found to be essential for stabilizing and reducing biosynthesized AgNPs and were associated with the organic substances of the leaf extract on the surfaces of *Mc-AgNPs* [81].

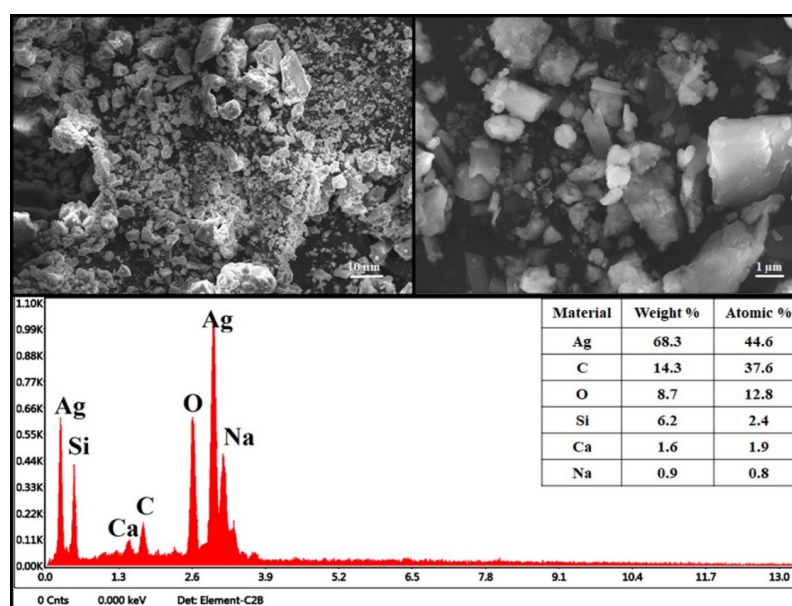


Figure 5. SEM and EDX analysis of *Mc-AgNPs*.

3.3.5. HR-TEM with SAED Analysis

Figure 6A displays the HR-TEM analysis of *Mc*-AgNPs. Most of the nanoparticles had a spherical shape in their morphology. It was discovered that some of the nanoparticles had an oval or elliptical shape. It is uncommon for biological systems to produce nanoparticles with varying degrees of sphericity and dimensionality. The noticeable distinction of lighter edges compared to the centers of the particles led researchers to hypothesize that proteins or other biomolecules enveloped the Ag nanoparticles [82]. HR-TEM examination revealed that most particles had a size of around 16 to 22 nm. Figure 6B presents an overview of the SAED pattern for the *Mc*-AgNPs. The synthesized silver nanoparticle (AgNP) crystallinity was confirmed through selected area electron diffraction (SAED) pattern analysis. The diffraction rings observed in the SAED patterns corresponded to the (111), (200), (220), and (311) planes, which are indicative of the fcc lattice structure commonly associated with *Mc*-AgNPs. This observation perfectly correlated with the XRD results, underscoring the spherical and crystalline nature of the NPs. High-resolution SAED images further substantiated the crystalline structure of the AgNPs, as demonstrated by the clear and consistent diffraction patterns across multiple magnifications [83].

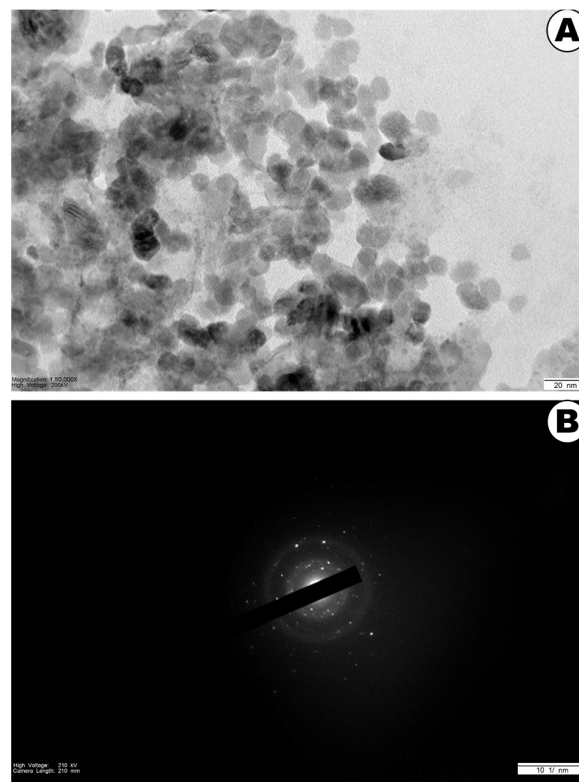


Figure 6. (A) HRTEM analysis for *Mc*-AgNPs (the synthesized nanoparticle was a cluster in morphology and highly agglomerated); (B) SAED analysis of *Mc*-AgNPs.

3.4. DPPH Assay

The antioxidant capacities of *Mc*-AgNPs were assessed using the DPPH assay. It is understood that DPPH-scavenging activities are related to hydrogen's ability to donate to different antioxidant molecules. Figure 7 depicts how the behavior of DPPH in radical scavenging is affected by various *Mc*-AgNP concentrations. *Mc*-AgNPs and ascorbic acid produced a potent inhibitory activity against DPPH radicals, a source of antioxidants. With higher concentrations, *Mc*-AgNPs' free radical scavenging ability seems to improve. Notably, at 1000 $\mu\text{g}/\text{mL}$, *Mc*-AgNPs showed more decisive antioxidant action, with a 67.77% inhibition rate, compared to ascorbic acid at 73.31%. Previous research has also indicated that as treatment doses are increased, antioxidant activity progressively rises [84–86]. As a result, the potential antioxidant capability of our synthesized *Mc*-AgNPs was evident.

Examining the ability of nanoparticles to quench neutrals revealed that *Mc*-AgNPs could produce free, stable neutral radicals from DPPH. Different facets of the antioxidant process were highlighted in the experimental investigations used. The DPPH assay showed that AgNPs donate electrons to neutralize the free radicals of unstable DPPH within the reaction medium [87].

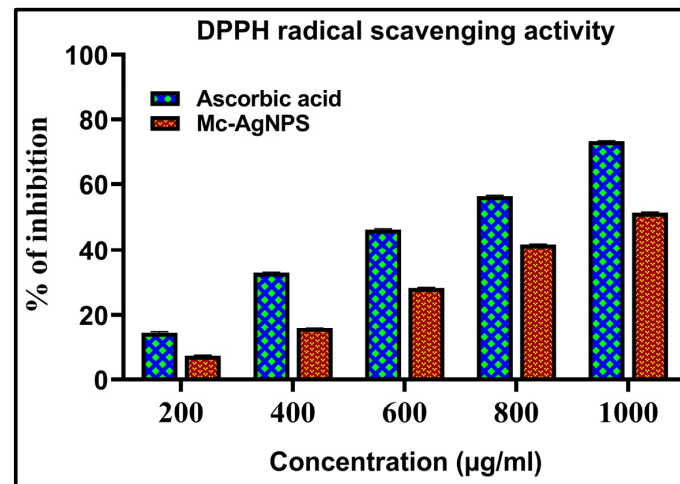


Figure 7. DPPH analysis of green synthesized *Mc*-AgNPs.

3.5. Cytotoxicity Activity

The cytotoxic effects of *Mc*-AgNPs were investigated on both MCF-7 cells and Vero cells. *Mc*-AgNPs had a dose-dependent cytotoxic impact on breast cancer cells. The IC_{50} values were 54.89 µg/mL for MCF-7 breast cancer cells and 160.74 µg/mL for the non-malignant Vero cells. Cytotoxicity assays indicated that *Mc*-AgNPs are more cytotoxic to cancer cells than to non-tumorigenic cells. Doxorubicin, used as a comparative standard, exhibited IC_{50} values of 2.04 µg/mL for MCF-7 cells and 3.08 µg/mL for Vero cells, as depicted in Figures 8 and 9 [88,89]. Likewise, the leaf extract of the *A. vulgaris*-mediated synthesis of AgNPs (*AV*-AgNPs) demonstrated an IC_{50} value of approximately 60 µg/mL for MCF-7 cells [87]. Due to improved cellular uptake and the retention of nanoparticles, *Cp*-AgNPs demonstrated a cytotoxicity gap in MCF-7 cell lines [90]. Despite their small size, nanoparticles resist P-glycoprotein efflux and can enter cells via endocytosis [91].

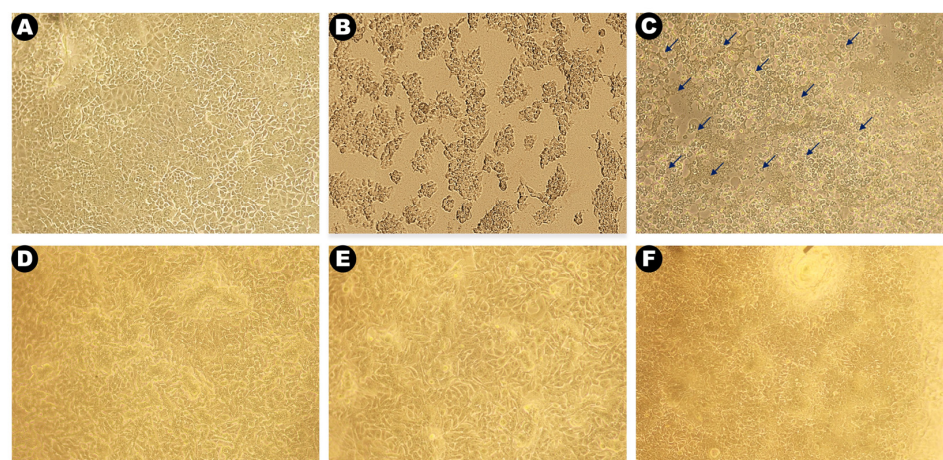


Figure 8. Anticancer activity of green synthesized *Mc*-AgNPs. (A) MCF-7 control; (B) MCF-7 treated with doxorubicin; (C) MCF-7 treated with *Mc*-AgNPs; (D) Vero cell line control, and (E) Vero cell line treated with doxorubicin; (F) Vero cell line treated with *Mc*-AgNPs.

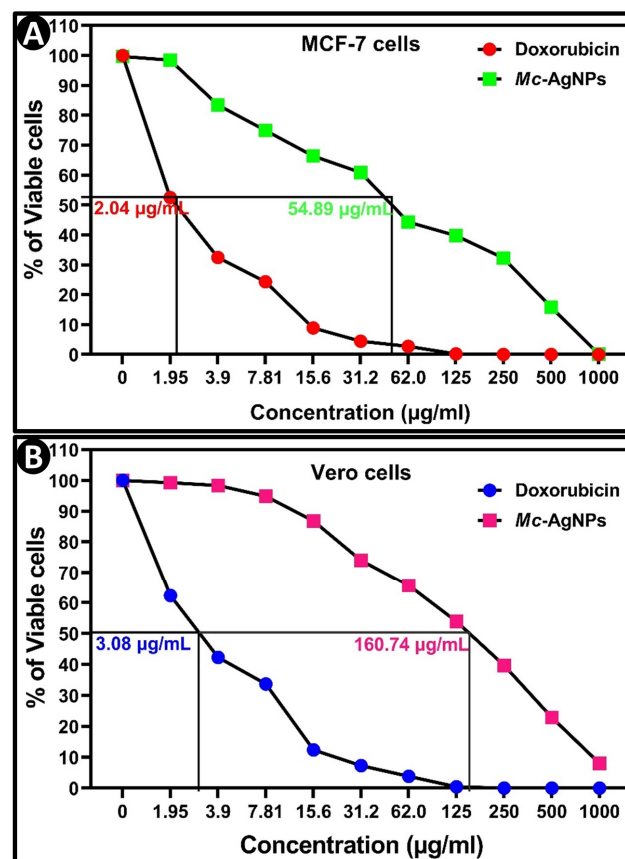


Figure 9. Determination of the IC_{50} value for *Mc-AgNPs* and Dox via an MTT assay; (A) MCF-7 cells (B) Vero cells.

3.6. Antibacterial Activity

Multi-drug resistance has been a significant obstacle to promising antibiotic therapeutics and necessitates the development of a medication with nanoforumulations to tackle resistant bacterial strains [92]. In this study, the antibacterial activity of biosynthesized *Mc-AgNPs* was evaluated by using the well-diffusion method, against a selection of four bacterial pathogens: Gram-positive (*E. coli* ATCC-25922, and *S. marcescens* ATCC-27137) and Gram-negative (MRSA ATCC-43300, and VREF ATCC-49624). Concerning the zone of inhibition for each strain of bacteria, *Mc-AgNPs* exhibited a significant level of inhibition of *E. coli*, followed by *S. marcescens*, MRSA, and VREF, respectively. The maximum zone of inhibition observed for *E. coli* at the highest dose of *Mc-AgNPs* was 17.33 mm (Figure 10). *Mc-AgNPs* exhibited dose-dependent antibacterial efficacy against all the bacterial pathogens. In the present study, the inhibitory action of *Mc-AgNPs* was comparatively low for Gram-negative bacteria. This difference in susceptibility is often attributed to the structural variations in the cell walls of these two types of bacteria [93]. Gram-positive bacteria have a thick peptidoglycan layer in their cell walls, making them more susceptible to the action of nanoparticles. On the other hand, Gram-negative bacteria have a thinner peptidoglycan layer and an outer membrane made up of LPS, lipoproteins, and phospholipids that act as a penetration barrier and only permit the entry of macromolecules [94]. The silver ions from the nanoparticles are attracted to the negative charge of the bacterial cell wall. When they encounter electrostatic attraction, they migrate and bind to the bacterial cell wall, influencing the permeability of the cell wall and altering its structure [75]. The DNA of microorganisms loses its ability to replicate and to produce cellular proteins, such as ribosome subunits. After exposure to Ag^+ ions, most of the enzymes necessary to produce ATP become inactive [95]. In our study, chloramphenicol was used as a positive control. The synthesized *Mc-AgNPs* had low antibacterial efficacy, when compared to

chloramphenicol. Contreras and Vazquez (1977) reported that chloramphenicol inhibited translation by preventing the peptidyl transferase reaction or translocation step on the 50S component of the bacterial ribosome [96].

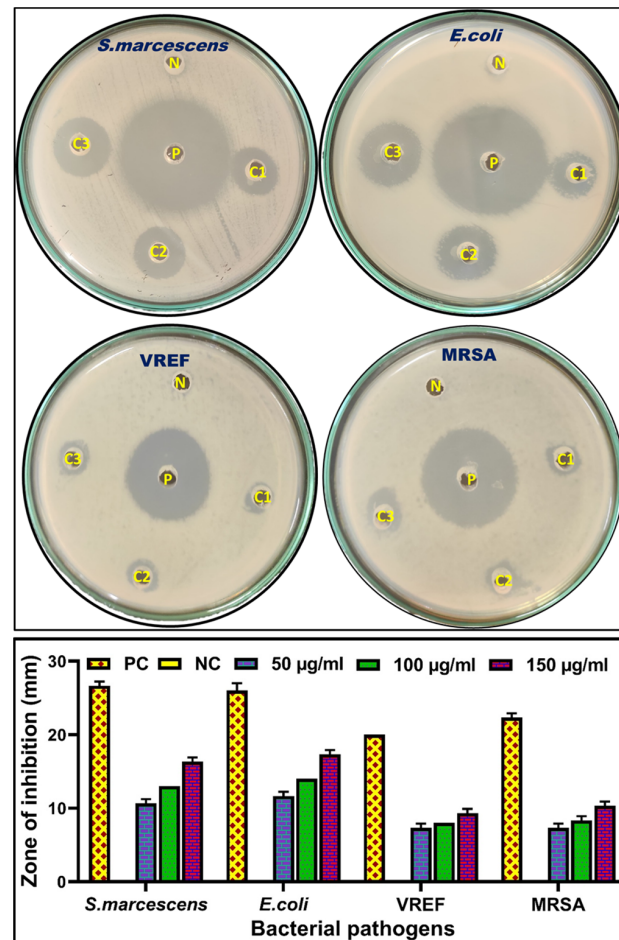


Figure 10. Antibacterial activity of green synthesized *Mc*-AgNPs against different clinical pathogenic bacteria.

Microbial Growth Assay

Microbial growth assays were conducted to evaluate the bactericidal activity of *Mc*-AgNPs against MRSA, VREF, *E. coli*, and *S. marcescens*. Bacterial isolates, numbering approximately 10^7 colony-forming units (CFUs), were exposed to varying concentrations of Ag-NPs (100, 80, 60, 40, and 20 µg/mL) and cultured on Mueller-Hinton agar (MHA) plates. Following treatment, a notable reduction in the colony count was observed for all four pathogens after 24 h, particularly with concentrations of 60 and 80 µg/mL of *Mc*-AgNPs. The observed reduction in colony numbers suggests the bactericidal efficacy of AgNPs against the tested microbial strains (Figure 11). The mechanism of action of *Mc*-AgNPs involves anchoring to the bacterial cell wall at multiple sites, followed by penetration and the induction of structural changes. This process leads to cell wall perforations, resulting in intracellular substance leakage [97]. Dizaj et al. (2014) suggested that AgNPs interact with the cell wall, causing disruptive effects [98]. Moreover, upon penetration, *Mc*-AgNPs release silver ions, which, in turn, generate reactive oxygen species. This oxidative stress affects membrane proteins and disrupts the electron transport chain [99]. The cumulative effect of these processes contributes to the observed bactericidal activity of *Mc*-AgNPs against bacteria, providing insights into their potential as antibacterial agents.

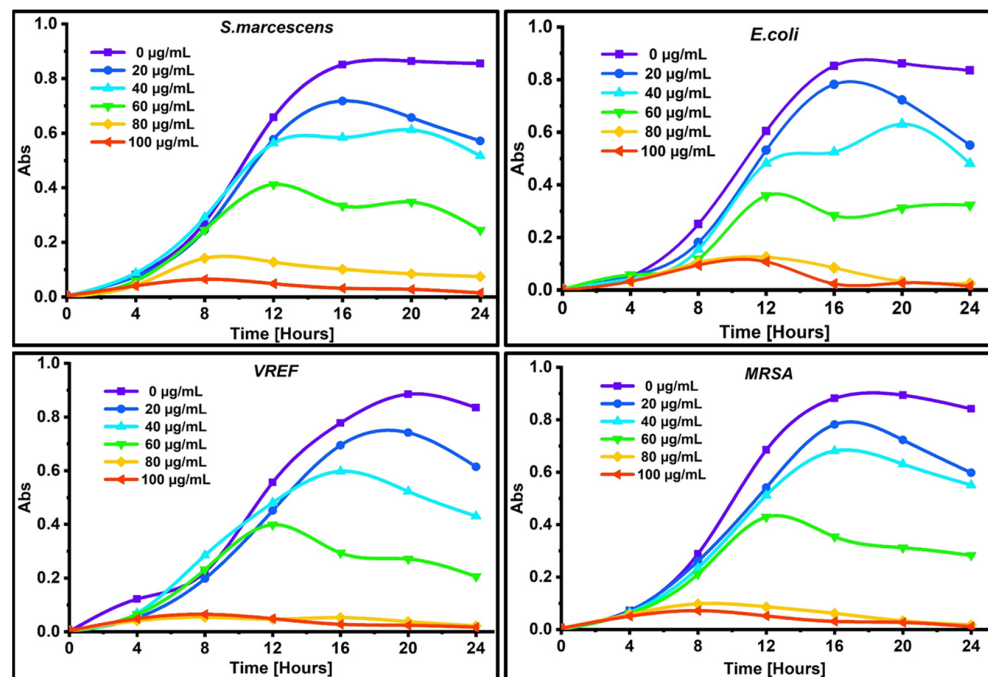


Figure 11. Microbial growth assay using *Mc-AgNPs*.

3.7. Photocatalytic Studies

For the past several years, the photocatalytic degradation of hazardous organic pollutants has drawn significant interest from researchers worldwide. Particularly toxic and non-biodegradable, colored organic dyes from the textile and paper industries harm the environment. Seventy percent of the dye material, sourced from azo dyes, severely pollutes the environment by dispersing potentially harmful particles into the aquatic system [100]. However, the conventional bio-treatment methods for degrading dye wastewater have recently been costly and ineffective due to the stability and aromatic complex structures of these organic dyes [101]. As a photocatalyst, metal oxide nanoparticles have shown remarkable effectiveness in mineralizing various environmental contaminants, including detergents, dyes, and volatile organic compounds [102]. Various metal oxides, such as Ag_2O , TiO_2 , ZnO , WO_3 , Fe_2O_3 , and CuO , have recently been used as essential photocatalysts for degrading organic dye pollutants in water and air [103].

The environmental concern of the photocatalytic nature and efficiency of the synthesized nanocomposite was evaluated effectively. Figure 12A shows the UV-Vis absorption spectra of an organic dye molecule, like methylene blue, when exposed to sunlight with a maximum light intensity of approximately 860–980 lux from 11.30 am to 2.30 pm. The sample solutions were collected at several time intervals, such as 0, 10, 30, 50, 70, 90, 120, and 180 min, in the presence of *Mc-AgNPs* nanocomposites as the photocatalysts. Decolorization was observed during the degradation study and may be due to damage to the sulfur-nitrogen bonds in the MB solution. After the degradation study, CO_2 and H_2O were formed along with degraded products. From the studies, the maximum photodegradation percentage obtained for methylene blue for each sample in the presence of the synthesized catalyst, *Mc-AgNPs*, was found to be around 60%. The photodegradation percentage values of MB dye in the presence of the *Mc-AgNPs* nanocomposites after 180 min of exposure are shown in Figure 12B. From Table 3, *Mc-AgNPs* have higher photocatalytic activity against M.B. dye than some other reported plant-mediated silver nanoparticles.

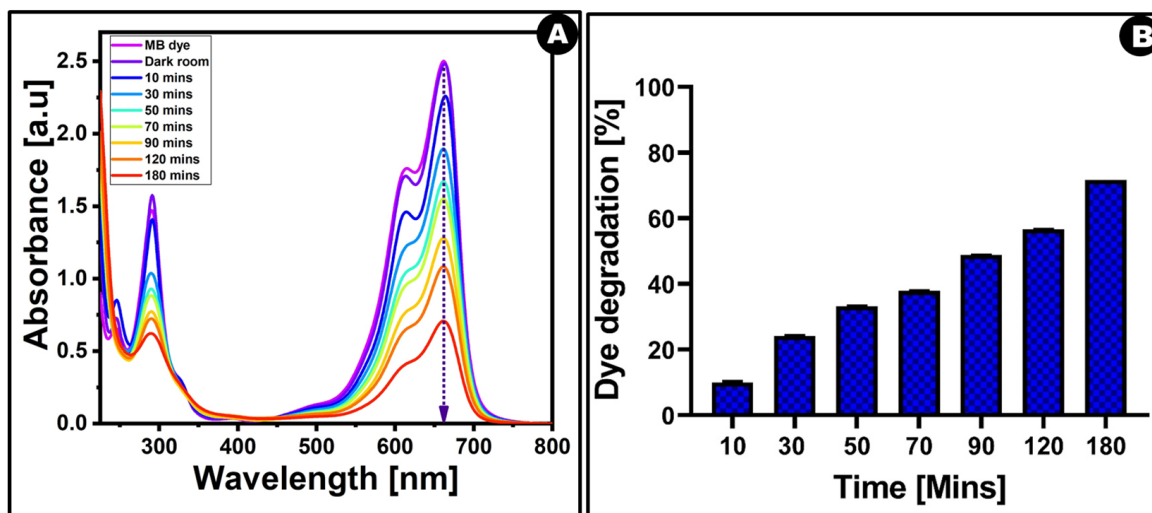
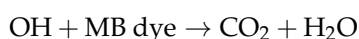
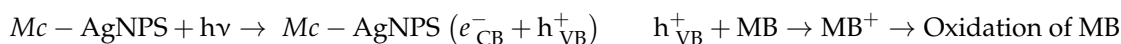


Figure 12. (A) Photocatalytic activity of green synthesized *Mc*-AgNPs; (B) Photodegradation of methylene blue dye in the presence of the green synthesized *Mc*-AgNPs.

Table 3. Comparison of photocatalytic activity of some silver nanoparticles against MB dye.

S.No	Catalyst	Pollutant	Degradation Efficiency (%) and Time	References
1	<i>Morinda tinctoria</i> -Ag	MB	95.3% & 72 h	[104]
2	Honey-Ag	MB	92% & 72 h	[105]
3	<i>Imperata cylindrical</i> -Ag	MB	92.06% & 14 min	[106]
4	<i>Gymnema sylvestre</i> -Ag	MB	95% & 7 h	[107]
5	<i>Peltophorum pterocarpum</i> -Ag	MB	82% & 6 min	[108]
6	<i>Camellia sinensis</i> -Ag	MB	95% & 72 h	[109]
7	<i>Momordica cymbalaria</i> -Ag	MB	60% & 3 h	Present work

The photocatalytic degradation process induces the degradation of MB. The destruction of MB was probable owing to the production of an electron and hole pair on the catalyst surface during light-source radiation. The electron and hole pair intermingled with a water molecule, generating hydroxyl radicals. This is accountable for breaking the harmful MB components. Electrons in the conduction band on the catalyst’s surface alter the molecular oxygen to superoxide ions and ultimately form hydrogen peroxide. The hole generates a hydroxyl radical, which plays an important role in the breakage of MB molecules [110].



Reusability Test and Stability Analysis of *Mc*-AgNPs

Regeneration and reusability are significant factors in the field of catalysis for an environmental friendly and cost-effective point of view. To evaluate the stability of the *Mc*-AgNPs, a reusability study was performed on the degradation of methylene blue dye. The catalyst was collected after the completion of the degradation study and washed, dried, and used for the reusability study. The degradation efficiency was slightly decreased during the degradation study and may be due to the loss of catalyst weight while washing and

drying. The degradation efficiency was found to be 60% in cycle I and gradually decreased after cycle IV, which was found to be 51%. Figure 13A shows the reusability study of the *Mc*-AgNPs against MB dye.

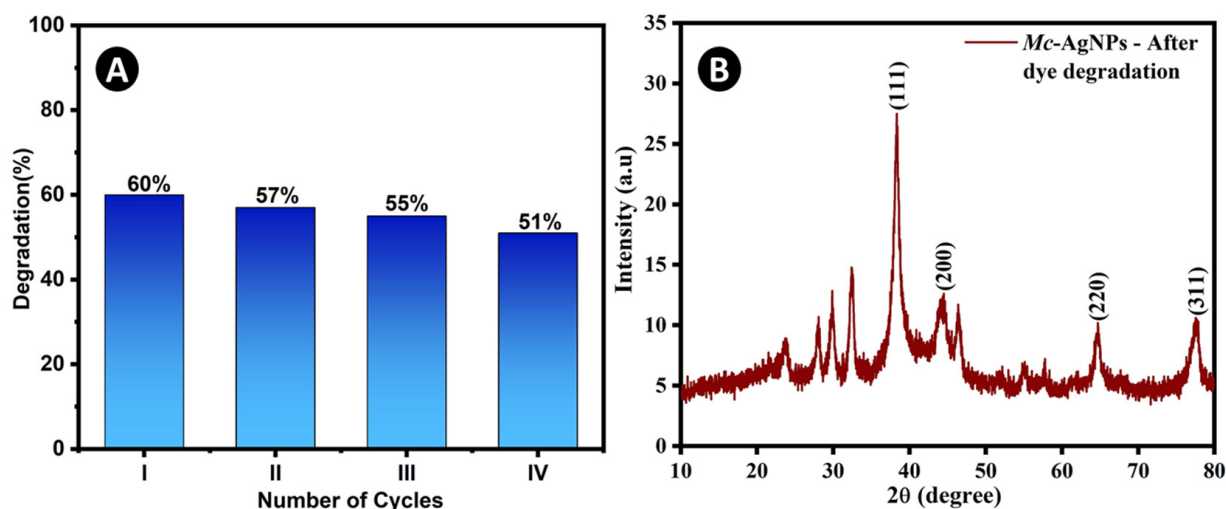


Figure 13. (A) Reusability test of *Mc*-AgNPs; (B) XRD analysis of *Mc*-AgNPs after recycling.

The *Mc*-AgNPs are moderately stable up to the IV cycle in the degradation of MB. However, the stability of the catalyst after the degradation process was investigated using XRD (Figure 13B). The results confirmed that the crystallinity of the *Mc*-AgNPs became lower, and impurity peaks appeared after the 4th cycle. This may be due to the catalyst's photo corrosion and photo dissolution.

4. Conclusions

In this study, an aqueous leaf extract from *M. cymbalaria* was successfully utilized to synthesize silver nanoparticles, where the extract plays an important role as a capping agent. In addition, the synthesized *Mc*-AgNPs show bacterial-inhibitory effects against MDR bacterial strains. The synthesized *Mc*-AgNPs exhibit potent scavenging properties and act as a defense activator against MCF-7 cells while exhibiting lower toxicity to *Mc*-AgNP-treated Vero cells. According to the results of the photocatalytic analysis, *Mc*-AgNPs were effective at degrading methylene blue dye when exposed to sunlight. As a result, the textile and water purification industries stand to gain a great deal from this. Our findings unequivocally corroborate the theory that plant-mediated nanoparticles will soon be able to be used as potent therapeutic agents against human pathogens to treat diseases brought on by free radicals and purify wastewater by eliminating harmful dyes.

Author Contributions: Conceptualization: M.S., G.R., S.P.K. and S.M.; Methodology: S.P.K. and S.M.; Investigation: M.S., G.R. and A.N.; Validation: M.S., G.R., and A.N.; Writing—Original draft preparation: M.S., G.R. and A.N.; Writing—review and editing: S.P.K. and S.M. All authors reviewed the results and approved the final version of the manuscript.

Funding: This research received no external funding.

Data Availability Statement: On request, the author will provide the data.

Conflicts of Interest: The authors declare no conflicts of interest.

References

1. He, X.; Deng, H.; Hwang, H.M. The current application of nanotechnology in food and agriculture. *J. Food Drug Anal.* **2019**, *27*, 1–21. [[CrossRef](#)] [[PubMed](#)]
2. Mariappan, V.; Vellasamy, K.M.; Mohamad, N.A.; Subramaniam, S.; Vadivelu, J. OneHealth approaches contribute towards antimicrobial resistance: Malaysian perspective. *Front. Microbiol.* **2021**, *12*, 718774. [[CrossRef](#)] [[PubMed](#)]
3. Shankar, P.R. Book review: Tackling drug-resistant infections globally. *Arch. Pharm. Pract.* **2016**, *7*, 110–111. [[CrossRef](#)]

4. Sánchez-López, E.; Gomes, D.; Esteruelas, G.; Bonilla, L.; Lopez-Machado, A.L.; Galindo, R.; Cano, A.; Espina, M.; Ettcheto, M.; Camins, A.; et al. Metal-based nanoparticles as antimicrobial agents: An overview. *Nanomaterials* **2020**, *10*, 292. [[CrossRef](#)] [[PubMed](#)]
5. Ferlay, J.; Colombet, M.; Soerjomataram, I.; Mathers, C.; Parkin, D.M.; Piñeros, M.; Znaor, A.; Bray, F. Estimating the global cancer incidence and mortality in 2018: GLOBOCAN sources and methods. *Int. J. Cancer* **2019**, *144*, 1941–1953. [[CrossRef](#)] [[PubMed](#)]
6. Curigliano, G.; Criscitiello, C. Successes and limitations of targeted cancer therapy in breast cancer. *Successes Limit. Target. Cancer Ther.* **2014**, *41*, 15–35.
7. Kumari, P.; Ghosh, B.; Biswas, S. Nanocarriers for cancer-targeted drug delivery. *J. Drug Target.* **2016**, *24*, 179–191. [[CrossRef](#)]
8. Tang, X.; Cai, S.; Zhang, R.; Liu, P.; Chen, H.; Zheng, Y.; Sun, L. Paclitaxel-loaded nanoparticles of star-shaped cholic acid-core PLA-TPGS copolymer for breast cancer treatment. *Nanoscale Res. Lett.* **2013**, *8*, 420. [[CrossRef](#)]
9. Abdalla, A.M.; Xiao, L.; Ullah, M.W.; Yu, M.; Ouyang, C.; Yang, G. Current challenges of cancer anti-angiogenic therapy and the promise of nanotherapeutics. *Theranostics* **2018**, *8*, 533. [[CrossRef](#)] [[PubMed](#)]
10. Khan, A.U.; Yuan, Q.; Khan, Z.U.H.; Ahmad, A.; Khan, F.U.; Tahir, K.; Shakeel, M.; Ullah, S. An eco-benign synthesis of AgNPs using aqueous extract of Longan fruit peel: Antiproliferative response against human breast cancer cell line MCF-7, antioxidant and photocatalytic deprivation of methylene blue. *J. Photochem. Photobiol. B Biol.* **2018**, *183*, 367–373. [[CrossRef](#)] [[PubMed](#)]
11. Alsukaibi, A.K. Various approaches for the detoxification of toxic dyes in wastewater. *Processes* **2022**, *10*, 1968. [[CrossRef](#)]
12. Khan, A.U.; Yuan, Q.; Wei, Y.; Tahir, K.; Khan, S.U.; Ahmad, A.; Khan, S.; Nazir, S.; Khan, F.U. Ultra-efficient photocatalytic deprivation of methylene blue and biological activities of biogenic silver nanoparticles. *J. Photochem. Photobiol. B Biol.* **2016**, *159*, 49–58. [[CrossRef](#)]
13. Narayan, N.; Meiyazhagan, A.; Vajtai, R. Metal nanoparticles as green catalysts. *Materials* **2019**, *12*, 3602. [[CrossRef](#)]
14. Tanase, C.; Berta, L.; Coman, N.A.; Roșca, I.; Man, A.; Toma, F.; Mocan, A.; Jakab-Farkas, L.; Biró, D.; Mare, A. Investigation of in vitro antioxidant and antibacterial potential of silver nanoparticles obtained by biosynthesis using beech bark extract. *Antioxidants* **2019**, *8*, 459. [[CrossRef](#)]
15. Behboodi, S.; Baghbani-Arani, F.; Abdalan, S.; Sadat Shandiz, S.A. Green engineered biomolecule-capped silver nanoparticles fabricated from *Cichorium intybus* extract: In vitro assessment on apoptosis properties toward human breast cancer (MCF-7) cells. *Biol. Trace Elem. Res.* **2019**, *187*, 392–402. [[CrossRef](#)] [[PubMed](#)]
16. Alqudami, A.; Annapoorni, S. Fluorescence from metallic silver and iron nanoparticles prepared by exploding wire technique. *Plasmonics* **2007**, *2*, 5–13. [[CrossRef](#)]
17. Jyoti, K.; Baunthiyal, M.; Singh, A. Characterization of silver nanoparticles synthesized using *Urtica dioica* Linn. leaves and their synergistic effects with antibiotics. *J. Radiat. Res. Appl. Sci.* **2016**, *9*, 217–227. [[CrossRef](#)]
18. Sharma, N.K.; Vishwakarma, J.; Rai, S.; Alomar, T.S.; AlMasoud, N.; Bhattarai, A. Green route synthesis and characterization techniques of silver nanoparticles and their biological adeptness. *ACS Omega* **2022**, *7*, 27004–27020. [[CrossRef](#)] [[PubMed](#)]
19. Gengan, R.M.; Anand, K.; Phulukdaree, A.; Chuturgoon, A. A549 lung cell line activity of biosynthesized silver nanoparticles using *Albizia adianthifolia* leaf. *Colloids Surf. B Biointerfaces* **2013**, *105*, 87–91. [[CrossRef](#)] [[PubMed](#)]
20. Kumar, D.; Kumar, P.; Singh, H.; Agrawal, V. Biocontrol of mosquito vectors through herbal-derived silver nanoparticles: Prospects and challenges. *Environ. Sci. Pollut. Res.* **2020**, *27*, 25987–26024. [[CrossRef](#)] [[PubMed](#)]
21. Adeyemi, J.O.; Oriola, A.O.; Onwudiwe, D.C.; Oyediji, A.O. Plant extracts mediated metal-based nanoparticles: Synthesis and biological applications. *Biomolecules* **2022**, *12*, 627. [[CrossRef](#)]
22. Rajan, R.; Chandran, K.; Harper, S.L.; Yun, S.I.; Kalaichelvan, P.T. Plant extract synthesized silver nanoparticles: An ongoing source of novel biocompatible materials. *Ind. Crops Prod.* **2015**, *70*, 356–373. [[CrossRef](#)]
23. Jeyadevi, R.A.; Sivasudha, T.; Rameshkumar, A.; Sangeetha, B.; Ananth, D.A.; Aseervatham, G.S.B. Nutritional constituents and medicinal values of *Momordica cymbalaria* (Athalakkai)—A review. *Asian Pac. J. Trop. Biomed.* **2012**, *2*, S456–S461. [[CrossRef](#)]
24. Gopu, C.; Chirumamilla, P.; Kagithoju, S.; Taduri, S. Green synthesis of silver nanoparticles using *Momordica cymbalaria* aqueous leaf extracts and screening of their antimicrobial activity: AgNPs studies in *Momordica cymbalaria*. *Proc. Natl. Acad. Sci. India Sect. B Biol. Sci.* **2022**, *92*, 771–782. [[CrossRef](#)]
25. Sundar, M.; Suresh, S.; Lingakumar, K. Influence of *Caralluma adscendens* Var. *attenuata* cold cream on UV-B damaged skin epidermal cells: A novel approach. *3 Biotech* **2021**, *11*, 155. [[CrossRef](#)]
26. Anand, T.; Sundararajan, M.; Anbukkarasi, M.; Thomas, P.A.; Geraldine, P.A. methanolic extract of *Ocimum basilicum* exhibits antioxidant effects and prevents selenite-induced cataract formation in cultured lenses of Wistar rats. *Pharmacogn. J.* **2019**, *11*, 496–504. [[CrossRef](#)]
27. Swamy, M.K.; Akhtar, M.S.; Mohanty, S.K.; Sinniah, U.R. Synthesis and characterization of silver nanoparticles using fruit extract of *Momordica cymbalaria* and assessment of their in vitro antimicrobial, antioxidant and cytotoxicity activities. *Spectrochim. Acta A Mol. Biomol. Spectrosc.* **2015**, *151*, 939–944. [[CrossRef](#)] [[PubMed](#)]
28. Jha, D.K.; Koneri, R.; Samaddar, S. Potential bio-resources of *Momordica dioica* roxb: A review. *Int. J. Pharm. Sci. Rev. Res.* **2017**, *45*, 203–209.
29. Kumar, A.; Dubey, A.; Singh, R. Investigation on Anti-Ulcer Activity of *Momordica dioica* Fruits in Wistar Rat. *Int. J. Res. Appl. Sci. Biotechnol.* **2022**, *9*, 105–111. [[CrossRef](#)]
30. Choudhary, B.R.; Berwal, M.K.; Ram, H.; Choudhary, M.K.; Singh, D. *Momordica balsamina* L.: An unexploited vegetable crop rich in medicinal and nutritional properties. *J. Agric. Ecol.* **2022**, *14*, 84–92. [[CrossRef](#)]

31. Elangovan, A.; Subramanian, A.; Durairaj, S.; Ramachandran, J.; Lakshmanan, D.K.; Ravichandran, G.; Nambirajan, G.; Thilagar, S. Antidiabetic and hypolipidemic efficacy of skin and seed extracts of *Momordica cymbalaria* on alloxan induced diabetic model in rats. *J. Ethnopharmacol.* **2019**, *241*, 111989. [[CrossRef](#)]
32. Ramesh, M.; Rao, Y.N.; Rao, A.A.; Prabhakar, M.C.; Rao, C.S.; Muralidhar, N.; Reddy, B.M. Antinociceptive and anti-inflammatory activity of a flavonoid isolated from *Caralluma attenuata*. *J. Ethnopharmacol.* **1998**, *62*, 63–66. [[CrossRef](#)]
33. Jia, R.B.; Wu, J.; Li, Z.R.; Ou, Z.R.; Lin, L.; Sun, B.; Zhao, M. Structural characterization of polysaccharides from three seaweed species and their hypoglycemic and hypolipidemic activities in type 2 diabetic rats. *Int. J. Biol. Macromol.* **2020**, *155*, 1040–1049. [[CrossRef](#)]
34. Jain, A.; Soni, M.; Deb, L.; Jain, A.; Rout, S.P.; Gupta, V.B.; Krishna, K.L. Antioxidant and hepatoprotective activity of ethanolic and aqueous extracts of *Momordica dioica* Roxb. leaves. *J. Ethnopharmacol.* **2008**, *115*, 61–66. [[CrossRef](#)]
35. Jha, D.K.; Koneri, R.; Samaddar, S. Medicinal use of an ancient herb *Momordica cymbalaria*: A review. *Int. J. Pharm. Sci. Res.* **2018**, *9*, 432–441.
36. Ahn, E.Y.; Jin, H.; Park, Y. Assessing the antioxidant, cytotoxic, apoptotic and wound healing properties of silver nanoparticles green-synthesized by plant extracts. *Mater. Sci. Eng. C* **2019**, *101*, 204–216. [[CrossRef](#)] [[PubMed](#)]
37. Fahimirad, S.; Ajallouei, F.; Ghorbanpour, M. Synthesis and therapeutic potential of silver nanomaterials derived from plant extracts. *Ecotoxicol. Environ. Saf.* **2019**, *168*, 260–278. [[CrossRef](#)] [[PubMed](#)]
38. Haggag, E.G.; Elshamy, A.M.; Rabeh, M.A.; Gabr, N.M.; Salem, M.; Youssif, K.A.; Samir, A.; Bin Muhsinah, A.; Alsayari, A.; Abdelmohsen, U.R. Antiviral potential of green synthesized silver nanoparticles of *Lampranthus coccineus* and *Malephora lutea*. *Int. J. Nanomed.* **2019**, *14*, 6217–6229. [[CrossRef](#)] [[PubMed](#)]
39. Totaro, P.; Rambaldini, M. Efficacy of antimicrobial activity of slow release silver nanoparticles dressing in post-cardiac surgery mediastinitis. *Interact. Cardiovasc. Thorac. Surg.* **2009**, *8*, 153–154. [[CrossRef](#)] [[PubMed](#)]
40. Bobo, D.; Robinson, K.J.; Islam, J.; Thurecht, K.J.; Corrie, S.R. Nanoparticle-based medicines: A review of FDA-approved materials and clinical trials to date. *Pharm. Res.* **2016**, *33*, 2373–2387. [[CrossRef](#)]
41. Buniyamin, I.; Akhir, R.M.; Asli, N.A.; Khusaimi, Z.; Malek, M.F.; Mahmood, M.R. Nanotechnology applications in biomedical systems. *Curr. Nanomater.* **2022**, *7*, 167–180. [[CrossRef](#)]
42. Waghchaure, R.H.; Adole, V.A. Biosynthesis of metal and metal oxide nanoparticles using various parts of plants for antibacterial, antifungal and anticancer activity: A review. *J. Indian Chem. Soc.* **2023**, *100*, 100987. [[CrossRef](#)]
43. Chandrasekharan, S.; Chinnasamy, G.; Bhatnagar, S. Sustainable phyto-fabrication of silver nanoparticles using *Gmelina arborea* exhibit antimicrobial and biofilm inhibition activity. *Sci. Rep.* **2022**, *12*, 156. [[CrossRef](#)] [[PubMed](#)]
44. Shreyash, N.; Bajpai, S.; Khan, M.A.; Vijay, Y.; Tiwary, S.K.; Sonker, M. Green synthesis of nanoparticles and their biomedical applications: A review. *ACS Appl. Nano Mater.* **2021**, *4*, 11428–11457. [[CrossRef](#)]
45. Jabeen, S.; Qureshi, R.; Munazir, M.; Maqsood, M.; Munir, M.; Shah, S.S.H.; Rahim, B.Z. Application of green synthesized silver nanoparticles in cancer treatment—A critical review. *Mater. Res. Express* **2021**, *8*, 092001. [[CrossRef](#)]
46. Sanpui, P.; Chattopadhyay, A.; Ghosh, S.S. Induction of apoptosis in cancer cells at low silver nanoparticle concentrations using chitosan nanocarrier. *ACS Appl. Mater. Interfaces* **2011**, *3*, 218–228. [[CrossRef](#)] [[PubMed](#)]
47. Kumar, H.; Bhardwaj, K.; Nepovimova, E.; Kuča, K.; Singh Dhanjal, D.; Bhardwaj, S.; Bhatia, S.K.; Verma, R.; Kumar, D. Antioxidant functionalized nanoparticles: A combat against oxidative stress. *Nanomaterials* **2020**, *10*, 1334. [[CrossRef](#)] [[PubMed](#)]
48. Kashyap, B.K.; Singh, V.V.; Solanki, M.K.; Kumar, A.; Ruokolainen, J.; Kesari, K.K. Smart Nanomaterials in Cancer Theranostics: Challenges and Opportunities. *ACS Omega* **2023**, *8*, 14290–14320. [[CrossRef](#)] [[PubMed](#)]
49. Saravanan, H.; Subramani, T.; Rajaramon, S.; David, H.; Sajeevan, A.; Sujith, S.; Solomon, A.P. Exploring nanocomposites for controlling infectious microorganisms: Charting the path forward in antimicrobial strategies. *Front. Pharmacol.* **2023**, *14*, 1282073. [[CrossRef](#)] [[PubMed](#)]
50. Zykova, M.V.; Volikov, A.B.; Buyko, E.E.; Bratishko, K.A.; Ivanov, V.V.; Konstantinov, A.I.; Logvinova, L.A.; Mihalyov, D.A.; Sobolev, N.A.; Zhirkova, A.M.; et al. Enhanced Antioxidant Activity and Reduced Cytotoxicity of Silver Nanoparticles Stabilized by Different Humic Materials. *Polymers* **2023**, *15*, 3386. [[CrossRef](#)]
51. Wagner, H. *Pharmazeutische Biologie AUF1*; Gustav Fisher Verlag: Stuttgart, Germany, 1993; p. 184, 15 BN 3-437-20 498-X.
52. Harborne, J.B.; Williams, C.A. Anthocyanins and other flavonoids. *Nat. Prod. Rep.* **1998**, *15*, 631–652. [[CrossRef](#)]
53. Little, E.; Ramakrishnan, M.; Roy, B.; Gazit, G.; Lee, A.S. The glucose-regulated proteins (GRP78 and GRP94): Functions, gene regulation, and applications. *Crit. Rev. Eukaryot. Gene Expr.* **1994**, *4*, 1–18. [[CrossRef](#)]
54. Raaman, N. *Phytochemical Techniques*; New India Publishing: Pitampura, India, 2006.
55. Kokate, C.K.; Purohit, A.P.; Gokhale, S.B. Pharmacognosy, Nirali Prakashan, Pune. *Med. J.* **2002**, *43*, 77–85.
56. Edeoga, H.O.; Okwu, D.E.; Mbaebie, B.O. Phytochemical constituents of some Nigerian medicinal plants. *Afr. J. Biotechnol.* **2005**, *4*, 685–688. [[CrossRef](#)]
57. Rajagopal, G.; Manivannan, N.; Sundararajan, M.; Kumar, A.G.; Senthilkumar, S.; Mathivanan, N.; Ilango, S. Biocompatibility assessment of silver chloride nanoparticles derived from *Padina gymnospora* and its therapeutic potential. *Nano Express* **2021**, *2*, 010010. [[CrossRef](#)]
58. Anand, T.; Anbukkarasi, M.; Thomas, P.A.; Geraldine, P.A. Comparison between plain eugenol and eugenol-loaded chitosan nanoparticles for prevention of in vitro selenite-induced cataractogenesis. *J. Drug Deliv. Sci. Technol.* **2021**, *65*, 102696. [[CrossRef](#)]

59. Rajagopal, G.; Nivetha, A.; Sundar, M.; Panneerselvam, T.; Murugesan, S.; Parasuraman, P.; Kumar, S.; Ilango, S.; Kunjiappan, S. Mixed phytochemicals mediated synthesis of copper nanoparticles for anticancer and larvicidal applications. *Heliyon* **2021**, *7*, e07360. [[CrossRef](#)]
60. Mosmann, T. Rapid colorimetric assay for cellular growth and survival: Application to proliferation and cytotoxicity assays. *J. Immunol. Methods* **1998**, *65*, 55–63. [[CrossRef](#)] [[PubMed](#)]
61. Rajagopal, G.; Nivetha, A.; Ilango, S.; Muthudevi, G.P.; Prabha, I.; Arthimhanju, R. Phytofabrication of selenium nanoparticles using *Azolla pinnata*: Evaluation of catalytic properties in oxidation, antioxidant and antimicrobial activities. *J. Environ. Chem. Eng.* **2021**, *9*, 105483. [[CrossRef](#)]
62. Kasithevar, M.; Saravanan, M.; Prakash, P.; Kumar, H.; Ovais, M.; Barabadi, H.; Shinwari, Z.K. Green synthesis of silver nanoparticles using *Alysicarpus monilifer* leaf extract and its antibacterial activity against MRSA and CoNS isolates in HIV patients. *J. Interdiscip. Nanomed.* **2017**, *2*, 131–141. [[CrossRef](#)]
63. Nivetha, A.; Prabha, I. Surfactant-Enhanced Nano Spinel Oxide for Applications in Catalysis, Dye Degradation and Antibacterial Activity. *ChemistrySelect* **2022**, *7*, e202202389. [[CrossRef](#)]
64. Dilika, F.; Bremner, P.D.; Meyer, J.J.M. Antibacterial activity of linoleic and oleic acids isolated from *Helichrysum pedunculatum*: A plant used during circumcision rites. *Fitoterapia* **2000**, *71*, 450–452. [[CrossRef](#)]
65. Abubacker, M.N.; Devi, P.K. In vitro antifungal potentials of bioactive compound oleic acid, 3-(octadecyloxy) propyl ester isolated from *Lepidagathis cristata* Willd. (*Acanthaceae*) inflorescence. *Asian Pac. J. Trop. Med.* **2014**, *7*, S190–S193. [[CrossRef](#)] [[PubMed](#)]
66. Habeeb Rahuman, H.B.; Dhandapani, R.; Narayanan, S.; Palanivel, V.; Paramasivam, R.; Subbarayalu, R.; Thangavelu, S.; Muthupandian, S. Medicinal plants mediated the green synthesis of silver nanoparticles and their biomedical applications. *IET Nanobiotechnol.* **2022**, *16*, 115–144. [[CrossRef](#)]
67. De Carvalho, C.C.; Caramujo, M.J. The various roles of fatty acids. *Molecules* **2018**, *23*, 2583. [[CrossRef](#)] [[PubMed](#)]
68. Sundar, M.; Lingakumar, K. Investigating the efficacy of topical application of *Ipomoea carnea* herbal cream in preventing skin damage induced by UVB radiation in a rat model. *Heliyon* **2023**, *9*, e19161. [[CrossRef](#)]
69. Zhang, L.; Zhang, W.; Zhang, F.; Jiang, J. Xylo-oligosaccharides and lignin production from *Camellia oleifera* shell by malic acid hydrolysis at mild conditions. *Bioresour. Technol.* **2021**, *341*, 125897. [[CrossRef](#)] [[PubMed](#)]
70. Mukherjee, P.K.; Singha, S.; Kar, A.; Chanda, J.; Banerjee, S.; Dasgupta, B.; Haldar, P.K.; Sharma, N. Therapeutic importance of Cucurbitaceae: A medicinally important family. *J. Ethnopharmacol.* **2022**, *282*, 114599. [[CrossRef](#)]
71. Mikhailova, E.O. Silver nanoparticles: Mechanism of action and probable bio-application. *J. Funct. Biomater.* **2020**, *11*, 84. [[CrossRef](#)]
72. Ansari, M.; Ahmed, S.; Abbasi, A.; Khan, M.T.; Subhan, M.; Bukhari, N.A.; Hatamleh, A.A.; Abdelsalam, N.R. Plant mediated fabrication of silver nanoparticles, process optimization, and impact on tomato plant. *Sci. Rep.* **2023**, *13*, 18048. [[CrossRef](#)]
73. Radzikowska-Büchner, E.; Flieger, W.; Pasiieczna-Patkowska, S.; Franus, W.; Panek, R.; Korona-Główniak, I.; Suśniak, K.; Rajtar, B.; Świątek, Ł.; Żuk, N.; et al. Antimicrobial and Apoptotic Efficacy of Plant-Mediated Silver Nanoparticles. *Molecules* **2023**, *28*, 5519. [[CrossRef](#)] [[PubMed](#)]
74. Bilal, M.; Rasheed, T.; Iqbal, H.M.; Li, C.; Hu, H.; Zhang, X. Development of silver nanoparticles loaded chi-tosan-alginate constructs with biomedical potentialities. *Int. J. Biol. Macromol.* **2017**, *105*, 393–400. [[CrossRef](#)] [[PubMed](#)]
75. Ahmed, S.; Ahmad, M.; Swami, B.L.; Ikram, S. Green synthesis of silver nanoparticles using *Azadirachta indica* aqueous leaf extract. *J. Radiat. Res. Appl. Sci.* **2016**, *9*, 1–7. [[CrossRef](#)]
76. Dipankar, C.; Murugan, S. The green synthesis, characterization and evaluation of the biological activities of silver nanoparticles synthesized from *Iresine herbstii* leaf aqueous extracts. *Colloids Surf. B Biointerfaces* **2012**, *98*, 112–119. [[CrossRef](#)] [[PubMed](#)]
77. Rajkuberan, C.; Prabukumar, S.; Sathishkumar, G.; Wilson, A.; Ravindran, K.; Sivaramakrishnan, S. Facile synthesis of silver nanoparticles using *Euphorbia antiqorum* L. latex extract and evaluation of their biomedical perspectives as anticancer agents. *J. Saudi Chem. Soc.* **2017**, *21*, 911–919. [[CrossRef](#)]
78. Veera, S.; Chirumamilla, P.; Dharavath, S.B.; Maduru, N.; Taduri, S. Facile green synthesis of silver nanoparticles using *Corallocarpus epigaeus* leaf extract: Structural, photoluminescence and antibacterial properties. *Chem. Data Collect.* **2023**, *45*, 101032. [[CrossRef](#)]
79. Jeeva, K.; Thiyagarajan, M.; Elangovan, V.; Geetha, N.; Venkatachalam, P. *Caesalpinia coriaria* leaf extracts mediated biosynthesis of metallic silver nanoparticles and their antibacterial activity against clinically isolated pathogens. *Ind. Crops Prod.* **2014**, *52*, 714–720. [[CrossRef](#)]
80. Sigamoney, M.; Shaik, S.; Govender, P.; Krishna, S.B.N. African leafy vegetables as bio-factories for silver nano-particles: A case study on *Amaranthus dubius* C Mart. Ex Thell. *S. Afr. J. Bot.* **2016**, *103*, 230–240. [[CrossRef](#)]
81. Jagtap, U.B.; Bapat, V.A. Green synthesis of silver nanoparticles using *Artocarpus heterophyllus* Lam. seed extract and its antibacterial activity. *Ind. Crops Prod.* **2013**, *46*, 132–137. [[CrossRef](#)]
82. Khan, M.J.; Shameli, K.; Sazili, A.Q.; Selamat, J.; Kumari, S. Rapid green synthesis and characterization of silver nanoparticles arbitrated by *curcumin* in an alkaline medium. *Molecules* **2019**, *24*, 719. [[CrossRef](#)]
83. Moond, M.; Singh, S.; Sangwan, S.; Devi, P.; Beniwal, A.; Rani, J.; Kumari, A.; Rani, S. Biosynthesis of silver nano-particles utilizing leaf extract of *Trigonella foenum-graecum* L. for catalytic dyes degradation and colorimetric sensing of Fe³⁺/Hg²⁺. *Molecules* **2023**, *28*, 951. [[CrossRef](#)] [[PubMed](#)]

84. Khuda, F.; Jamil, M.; Khalil, A.A.K.; Ullah, R.; Ullah, N.; Naureen, F.; Abbas, M.; Khan, M.S.; Ali, S.; Farooqi, H.M.U.; et al. Assessment of antioxidant and cytotoxic potential of silver nanoparticles synthesized from root extract of *Reynoutria japonica* Houtt. *Arab. J. Chem.* **2022**, *15*, 104327. [[CrossRef](#)]
85. Ajaykumar, A.P.; Sabira, O.; Binitha, V.S.; Varma, S.R.; Mathew, A.; Jayaraj, K.N.; Janish, P.A.; Zeena, K.V.; Sheena, P.; Venugopal, V.; et al. Bio-Fabricated Silver Nanoparticles from the Leaf Extract of the Poisonous Plant, *Holigarna arnottiana*: Assessment of Antimicrobial, Antimitotic, Anticancer, and Radical-Scavenging Properties. *Pharmaceutics* **2023**, *15*, 2468. [[CrossRef](#)] [[PubMed](#)]
86. Hamida, R.S.; Ali, M.A.; Alfassam, H.E.; Momenah, M.A.; Alkhateeb, M.A.; Bin-Meferij, M.M. One-Step Phytofabrication Method of Silver and Gold Nanoparticles Using *Haloxylon Salicornicum* for Anticancer, Antimicrobial, and Antioxidant Activities. *Pharmaceutics* **2023**, *15*, 529. [[CrossRef](#)] [[PubMed](#)]
87. Rasheed, T.; Bilal, M.; Iqbal, H.M.; Li, C. Green biosynthesis of silver nanoparticles using leaves extract of *Artemisia vulgaris* and their potential biomedical applications. *Colloids Surf. B Biointerfaces* **2017**, *158*, 408–415. [[CrossRef](#)] [[PubMed](#)]
88. Bordoni, V.; Sanna, L.; Lyu, W.; Avitabile, E.; Zoroddu, S.; Medici, S.; Kelvin, D.J.; Bagella, L. Silver nanoparticles derived by artemisia arborescens reveal anticancer and apoptosis-inducing effects. *Int. J. Mol. Sci.* **2021**, *22*, 8621. [[CrossRef](#)] [[PubMed](#)]
89. Mariadoss, A.V.A.; Ramachandran, V.; Shalini, V.; Agilan, B.; Franklin, J.H.; Sanjay, K.; Alaa, Y.G.; Tawfiq, M.A.A.; Ernest, D. Green synthesis, characterization and antibacterial activity of silver nanoparticles by *Malus domestica* and its cytotoxic effect on (MCF-7) cell line. *Microb. Pathog.* **2019**, *135*, 103609. [[CrossRef](#)]
90. Ingale, S.; Gaykar, B.; Pagar, K.; Shelke, D. Green Synthesis of Silver Nanoparticles from *Cyathocline purpurea* (Don) O. Kuntze and Its Efficacy Against MCF-7 Cancer Cell Line. *BioNanoScience* **2023**, *13*, 1197–1212. [[CrossRef](#)]
91. Halder, J.; Pradhan, D.; Kar, B.; Ghosh, G.; Rath, G. Nano therapeutics approaches to overcome P-glycoprotein-mediated multi-drug resistance in cancer. *Nanomed. NBM* **2022**, *40*, 102494. [[CrossRef](#)]
92. Odonkor, S.T.; Addo, K.K. Bacteria resistance to antibiotics: Recent trends and challenges. *Int. J. Biol. Med. Res.* **2011**, *2*, 1204–1210.
93. Khan, S.; Rukayadi, Y.; Jaafar, A.H.; Ahmad, N.H. Antibacterial potential of silver nanoparticles (SP-AgNPs) synthesized from *Syzygium polyanthum* (Wight) Walp. against selected foodborne pathogens. *Heliyon* **2023**, *9*, e22771. [[CrossRef](#)]
94. Netai, M.M.; Stephen, N.; Musekiwa, C. Synthesis of silver nanoparticles using wild *Cucumis anguria*: Characterization and antibacterial activity. *Afr. J. Biotechnol.* **2017**, *16*, 1911–1921.
95. Franci, G.; Falanga, A.; Galdiero, S.; Palomba, L.; Rai, M.; Morelli, G.; Galdiero, M. Silver nanoparticles as potential antibacterial agents. *Molecules* **2015**, *20*, 8856–8874. [[CrossRef](#)]
96. Contreras, A.; Vazquez, D. Cooperative and antagonistic interactions of peptidyl-tRNA and antibiotics with bacterial ribosomes. *Eur. J. Biochem.* **1977**, *74*, 539–547. [[CrossRef](#)]
97. Haseef, H.M.A.; Dinesh, S.; Prakash, J.; Marvaan, M.S.; Madasamy, S.; Pannerselvam, B.; Venkatasubbu, G.D. Calcium oxide/silica nanocomposite and *L. coromandelica* bark incorporated κ -carrageenan/sodium alginate hydrogel for rapid hemostasis. *Int. J. Biol. Macromol.* **2024**, *254*, 127951. [[CrossRef](#)] [[PubMed](#)]
98. Dizaj, S.M.; Lotfipour, F.; Barzegar-Jalali, M.; Zarrintan, M.H.; Adibkia, K. Antimicrobial activity of the metals and metal oxide nanoparticles. *Mater. Sci. Eng. C* **2014**, *44*, 278–284. [[CrossRef](#)] [[PubMed](#)]
99. Ahmed, S.; Ahmad, M.; Swami, B.L.; Ikram, S. A review on plants extract mediated synthesis of silver nanoparticles for antimicrobial applications: A green expertise. *J. Adv. Res.* **2016**, *7*, 17–28. [[CrossRef](#)] [[PubMed](#)]
100. Torkaman, M.; Moradi, R.; Keyvani, B. Photocatalytic degradation azo dye Direct Red 23 using carbon nanotubes particles by UV/H₂O₂ process in batch photoreactor. *Rev. Roum. Chim.* **2016**, *61*, 763–772.
101. Ismail, M.; Akhtar, K.; Khan, M.I.; Kamal, T.; Khan, M.A.; Asiri, A.; Seo, J.; Khan, S.B. Pollution, toxicity and carcinogenicity of organic dyes and their catalytic bio-remediation. *Curr. Pharm. Des.* **2019**, *25*, 3645–3663. [[CrossRef](#)]
102. Yogalakshmi, K.N.; Das, A.; Rani, G.; Jaswal, V.; Randhawa, J.S. Nano-bioremediation: A new age technology for the treatment of dyes in textile effluents. In *Bioremediation of Industrial Waste for Environmental Safety: Volume I: Industrial Waste and Its Management*; Springer: Berlin/Heidelberg, Germany, 2020; pp. 313–347.
103. Lidia, F.; Maria, H. TiO₂/Fly Ash nanocomposite for photodegradation of organic pollutant. In *Handbook of Nano-Materials and Nanocomposites for Energy and Environmental Applications*; Springer: Cham, Switzerland, 2020; pp. 1–24.
104. Vanaja, M.; Paulkumar, K.; Baburaja, M.; Rajeshkumar, S.; Gnanajobitha, G.; Malarkodi, C.; Sivakavinesan, M.; Annadurai, G. Degradation of methylene blue using biologically synthesized silver nanoparticles. *Bioinorg. Chem. Appl.* **2014**, *19*, 2014. [[CrossRef](#)]
105. Al-Zaban, M.I.; Mahmoud, M.A.; AlHarbi, M.A. Catalytic degradation of methylene blue using silver nanoparticles synthesized by honey. *Saudi J. Biol. Sci.* **2021**, *28*, 2007–2013. [[CrossRef](#)]
106. Fairuzi, A.A.; Bonnia, N.N.; Akhir, R.M.; Abrani, M.A.; Akil, H.M. 2018, January. Degradation of methylene blue using silver nanoparticles synthesized from *Imperata cylindrica* aqueous extract. *IOP Conf. Ser. Earth Environ. Sci.* **2018**, *105*, 012018. [[CrossRef](#)]
107. Kumar, M.S.; Supraja, N.; David, E. Photocatalytic degradation of methylene blue using silver nanoparticles synthesized from *Gymnema sylvestre* and antimicrobial assay. *Nov. Res. Sci.* **2019**, *2*, 1–7.
108. Ogundare, S.A.; Adesetan, T.O.; Muungani, G.; Moodley, V.; Amaku, J.F.; Atewolara-Odudu, O.C.; Yussuf, S.T.; Sanyaolu, N.O.; Ibikunle, A.A.; Balogun, M.S.; et al. Catalytic degradation of methylene blue dye and antibacterial activity of biosynthesized silver nanoparticles using *Peltophorum pterocarpum* (DC.) leaves. *Environ. Sci. Adv.* **2023**, *2*, 247–256. [[CrossRef](#)]

109. Trieu, Q.A.; Le, C.T.B.; Pham, C.M.; Bui, T.H. Photocatalytic degradation of methylene blue and antibacterial activity of silver nanoparticles synthesized from *Camellia sinensis* leaf extract. *J. Exp. Nanosci.* **2023**, *18*, 2225759. [[CrossRef](#)]
110. Alam, M.W.; Aamir, M.; Farhan, M.; Albulayyah, M.; Ahmad, M.M.; Ravikumar, C.R.; Dileep Kumar, V.G.; Ananda Murthy, H.C. Green synthesis of Ni-Cu-Zn based nanosized metal oxides for photocatalytic and sensor applications. *Crystals* **2021**, *11*, 1467. [[CrossRef](#)]

Disclaimer/Publisher's Note: The statements, opinions and data contained in all publications are solely those of the individual author(s) and contributor(s) and not of MDPI and/or the editor(s). MDPI and/or the editor(s) disclaim responsibility for any injury to people or property resulting from any ideas, methods, instructions or products referred to in the content.